



Interaction mechanisms and damage formation in laser cutting of CFRP laminates obtained by recycled carbon fibre

Claudio Leone^{1,3} · Emanuele Mingione¹ · Silvio Genna^{2,3}

Received: 15 February 2022 / Accepted: 30 April 2022 / Published online: 16 May 2022
© The Author(s) 2022, corrected publication 2022

Abstract

The increase in the use of composite materials poses the problem of their disposal/recycling after the End of Life (EOL). Different strategies were developed to recycle composite material, resulting in the availability of new raw materials, characterised by overall good mechanical properties and significantly low cost. However, the applicability of these materials to industrial production also depends on the possibility of producing and processing them with likewise available technologies. Among the production and processing technologies that can be adopted for recycled composite materials, resin infusion under flexible tooling (RIFT) and laser machining, respectively, stand out above all due to the high production/machining speed compared to the cost. This paper investigates the possibility to apply both these technologies to carbon fibre–reinforced polymer laminates obtained by adopting recycled carbon fibres. Recycled CFRP plates of about 2.7 mm in thickness were produced by RIFT and characterised in tensile and flexural tests. After mechanical characterisation, cutting tests were performed by using a 450 W QCW fibre laser, varying the pulse power, the pulse length, and the pulse overlap. The kerf geometries and the HAZ extension were measured at the upper and bottom parts as well as in the section. Analysis of variance was adopted to define which and how the process parameters affect the kerf dimension and HAZ extension. Results showed that it is possible to cut the composite at a cutting speed up to 2000 mm/s, obtaining, in the best conditions, narrow kerf, limited HAZ, and taper angle of about 0°.

Keywords Carbon fibre–reinforced composite · Recycled carbon fibre · Laser machining · Thermal damage

1 Introduction

In the last decade, carbon fibre–reinforced polymers (CFRP), thanks to their remarkable properties in terms of specific properties, fatigue, and environmental resistance, have been steadily increasing their applications in different fields, such as aerospace, automotive, train, boat, sports equipment, energy production, and prosthesis [1]. It has been estimated that in the next 10 years the carbon fibre (CF) market can roughly triple its turnover (about 4.7 billion USD in 2019

against the 13.3 billion in 2026 [2]). Although the use of CFRP provides several advantages, their use will lead to future new waste materials, increasing issues in terms of environmental impact. The CFRP wastes, such as industrial production scrap and End of Life (EOL) components, produced in the next years were estimated in [3]. They calculated the production of about 9-kilo tonnes in 2019 and estimated it the triple in 2027. Thus, it is necessary to develop new processes able to manage the CFRP wastes with minimal environmental impact. These processes involve not only the disposal/recovery methods of the CFRP components once the EoL is reached, but also the inclusion of recovered materials in a circular economy system.

Detailed descriptions of EOL alternative processes are in [4–6]. The authors evaluate different solutions, including landfill, incineration, mechanical recycling, chemical decomposition, fluidised bed, and pyrolysis fibre recovery processes. In [4], the authors concluded that to obtain an effective composite recovery, incentives, infrastructure, recycling techniques, and market commitment are required.

✉ Claudio Leone
claudio.leone@unicampania.it

¹ Department of Engineering, University of Campania Luigi Vanvitelli, via Roma 29, Aversa, CE 81031, Italy

² Department of Enterprise Engineering Mario Lucertini, University of Rome Tor Vergata, Via Del Politecnico 1, Rome 00133, Italy

³ CIRTIBS Research Centre, University of Naples Federico II, P.le Tecchio 80, Naples 80125, Italy

Witik et al. [5] indicate that, compared to energy recovery (i.e. incineration), the possibility to achieve effective benefits from fibre recovery depends on the impacts of the selected recovery process, and also the type of secondary application in which they are used. Naqvi et al. [6] highlighted that CFRC recovery is a global challenge since they must meet environmental factors, governmental legislation, production cost, and management of resources. However, they underline that to turn these composite wastes into a valuable resource, a circular economy must be created by closing the loop with a cradle-to-cradle approach. This involves different aspects, such as material source selection, recovering process, development low cost and large-scale production technologies, and processing technologies. Actually, carbon fibre recovering techniques can mainly be divided into two families: chemical decomposition and pyrolysis processes. The former adopts a solvent under supercritical conditions to decompose the polymer matrix leaving the fibres intact [4–15]. These processes are more suitable for the recovery of high-value fibres (typically pre-preg scrap) since they avoid fibre degradation and reclaim carbon fibres with high retained strength and clean surface. Conversely, pyrolysis techniques decompose the polymer matrix at sufficiently high temperatures (400–900 °C) in an atmosphere of nitrogen and oxygen gas [4–6, 16–23] and, compared to chemical decomposition, have lower costs. However, the pyrolysis method is an energy-consuming process, requires long times (typically 4–6 h), and results in both fibre damages as well as contamination [6, 21]. For the aforementioned reasons, this process is a viable technique for the recovery of low-value fibres (typically composite parts at their EOL) [24].

Many authors have proposed the adoption of recycled carbon fibres (rCFs) for concrete reinforcement in different industrial fields, which allows benefits in terms of environmental, financial, and mechanical properties [21, 25–31]. One of the sectors where this type of reinforcement has been extensively studied in the literature is the building constructions [21, 25–28]. Akbar and Liew [21, 26] found out that the adoption of the rCFs in cement composites greatly affects the mechanical properties and the environmental impact of the material. They reported an increase in elastic modulus, splitting tensile strength, and fracture toughness of up to 57%, 188%, and 325%, respectively. The environmental impact assessment revealed that with the addition of 1% of rCFs while replacing 10% of cement with silica fume, the overall global warming potential in terms of CO₂ emissions comes out to be 13.69% less than plain cement paste impact. Moreover, 22% of energy consumption and 70% of the cost can be saved by replacing the virgin carbon fibres (vCFs) with rCFs in the cement composites. Saccani et al. [25] have recycled wastes made of thermosets pre-preg scraps deriving from the production of epoxy-carbon fibre composites without any previous high temperature or chemical treatments as

reinforcement to produce building materials. An addition of 5% in volume of short-chopped fibres coated by resin on conventional Portland cement showed an increase in flexural strength and toughness. An extensive review of rCF applications in transportation fields is reported in [29]; the authors showed solutions for the recovery and re-use of recycled carbon fibre in automotive and railway industries, as well as in aviation and wind turbine constructions.

The interest of the scientific community in fibre recycling made many authors investigate different material properties [30, 31]. Genna et al. [30] adopted the resin infusion process to produce a composite laminate 4 mm in thickness with rCF under the form of non-woven fabric (mat) and carried out different mechanical properties, through quasi-static and dynamic tests. The tensile, the flexural, and the low-velocity impact loading behaviour were investigated considering, also, the influence of different stratifications on mechanical characteristics. A further issue regards the possibility to have low-cost and high-productivity manufacturing processes able to cut, drill, and machine new composite materials. Composite materials are difficult to machine with conventional cutting methods since they produce tool wear and damage, such as matrix degradation (due to the heat produced by friction), delamination, and fibre pull out [32–34]. Moreover, machining is not suitable when very small complex shapes are required. Compared to the conventional methods, water jet (WJ) and abrasive water jet (AWJ) machining show different advantages such as the absence of heat-affected zone (HAZ), and the elimination of dust by jet entrainment and high cutting speed [35]. However, both AW and AWJ have drawbacks such as moisture absorption, delamination, abrasive particle deposit (for AWJ), and slow effective cutting speed [35–38]. A possible alternative is represented by laser cutting (LC), which can be used on almost all categories of materials, including metals [39–45], ceramics [46–48], and composites [35, 49–60]. Compared to conventional cutting processes, laser cutting offers several advantages: it does not apply any mechanical force, absence of wear; it does not require complex fixtures; also, since the laser beam spot is very small, it is possible to realise complex shapes and accurate geometries with narrow kerfs, in a very short time [61]; in addition, compared to WJ and AWJ, laser machining shows lower kerfs width, higher process speed, and material removal rate [38].

However, laser cutting is a thermal process; therefore, thermal damage can occur (matrix recession and burning, fibre pull out, fibre swelling, delamination, etc.). Thermal damage and HAZ formations are a consequence of the difference between the carbon fibre and the epoxy matrix properties in terms of laser absorbance, degradation temperature, and thermal conductivity [35, 50, 51, 55–60, 62–65]. As a matter of fact, the composite matrix shows a low absorptivity at the wavelength range of about

1 μm ; in addition, either the energy required to evaporate or sublimate the carbon fibres and the thermal conductivity is more than one order of magnitude higher for the matrix [50, 51, 58, 63]. Then during the beam-material interaction, the time that elapses before the vaporisation condition for CF is larger than that for the resin [51, 55, 63, 64]. During this period, thanks to the good conductivity of the fibres, a great amount of heat is conducted through the carbon fibres and released into the matrix, producing matrix overheating [51, 62, 65, 66], comprised in the kerf neighbour. The latter results in matrix thermal degradation, the presence of fibres unbonded from the matrix, cavity, and delamination formation. Obviously, the thermal damages depend on the material characteristics (matrix, reinforcement type, reinforcement content and lay-up [56–58]), laser source (wavelength, continuous or pulsed mode, average power, etc. [56, 59, 60, 62, 67–70]), and the process parameters [50–52, 62–65].

This work aims to study the laser workability of a CFRP obtained by adopting recycled carbon fibres. CFRP plates 2.7 mm in thickness, made of recycled fibres, were produced by resin infusion under flexible tooling (RIFT) and characterised in tensile and flexural tests. Afterwards, laser cutting tests were carried out by way of a 450 W quasi-continuous wave (QCW) fibre laser in a pulsed regime, varying the pulse power, the pulse length, and the pulse overlap to optimise the cutting process (i.e. HAZ and kerf reduction and increase in the cutting speed). The kerf width dimensions (at the upper and bottom) and the HAZ extension (in different points) were measured in the section and on the external surfaces. Analysis of variance (ANOVA) was adopted to define which and how the process parameters affect the kerf dimension and HAZ extension. Results show that, with the adopted laser, it is possible to cut the composite at a cutting speed up to 2000 mm/s, obtaining, in the best conditions, a kerf of about 600 μm , a limited HAZ (300 μm) and a taper angle of about 0° . Results highlight that, by an appropriate selection of materials, production, and processing technologies, it is possible to obtain products characterised by good performance and low cost.

Moreover, comparing the measures acquired on the external surface to the section ones, the latter appears to be more suitable and reliable for the kerf characterisation.

2 Material, equipment, and procedures

2.1 Materials

CFRP plates, 2.7 mm in thickness, were produced through the resin infusion process adopting a rCF reinforcement, under the form of non-woven carbon fabric 200 g/m^2 (KARBOFELT by Karborek), obtained by the row, textile, prepreg, and CFRP scrap recycling by pyrolysis [71]. This material is a flexible insulating extremely compact felt with the shape of a mattress. It has good thermal insulating properties, and is highly resistant to temperature, extremely flexible, and compact [72]. In Fig. 1, images of the adopted carbon felt are reported. As a matrix, a 2-component modified epoxy system, SX8 EVO (by Mates), was adopted. This is a low viscosity matrix for laminating and infusion/injection processes. The very low viscosity guarantees the perfect impregnation of the carbon, glass, and aramid reinforcement even in the case of multi-axial or coupled to high grammage. Thanks to the low viscosity, this system is designed for all those processes that require maximum fluidity of the resin and is, therefore, often applied for injections, infusions, and machining RTM standard or light. In Table 1, the basic properties of the adopted matrix systems are reported.

2.2 Laser equipment

The experimental tests were performed adopting a CNC system (Rofin finecut Y 340) equipped with a 450 W quasi-continuous wave (QCW) Yb:YAG fibre laser (IPG YLR-450/4500-QCW-AC) working at the fundamental wavelength $\lambda = 1070$ nm. The laser source can work in both continuous wave (CW) and pulsed wave (PW). The maximum average power released by the laser is 450 W (P_a); but, in PW mode, it can release a pulse power (P_p) up to 4500 W. The only limitations are the following:

Fig. 1 Images of the recycled non-woven carbon fabric for: **a** non-woven carbon fabric at 35 \times ; **b** single fibre at 2500 \times

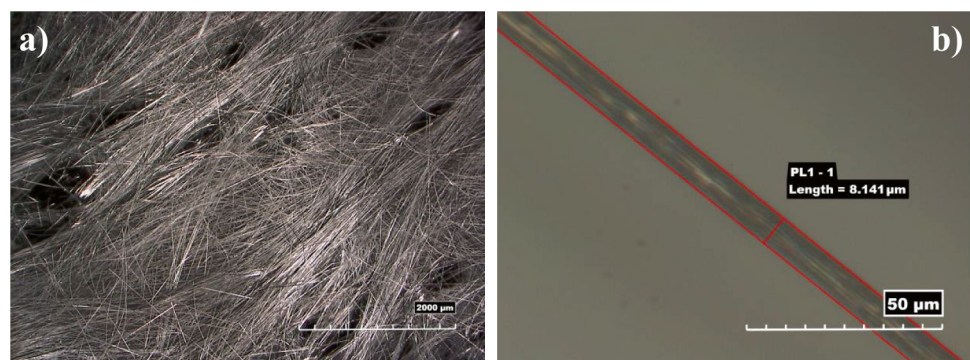


Table 1 SX8 EVO matrix properties

Characteristic	Unit	Matrix
Tensile strength (ASTM D 638)	MPa	65–75
Elongation at break (ASTM D 638)	%	6–7
Tensile Young's modulus (UNI5819)	GPa	2.4–3.0
Flexural strength (ASTM D 790)	MPa	95–110
Flexural modulus (ASTM D 790)	GPa	2.4–3.2
Shore (ASTM D 15)	–	86–90
Compressive strength (UNI 4279)	MPa	90–110
Glass transition temperature	°C	75–85
Water absorption 24 h at room temperature (ASTM D570)	%	0.1–0.2
Water absorption 2 h at 100 °C (ASTM D570)	%	0.6–0.7
Operating temperature	°C	90

the average power cannot exceed the nominal value in CW mode (450 W) and the duty cycle (δ) (i.e. the product of the frequency per pulse duration) cannot exceed 50%. Thus, considering the well-known equations for the average power calculation, pulse energy (E_p), pulse power, and duty cycle (δ) [73]:

$$E_p = P_a / f \quad (1)$$

$$P_p = E_p / D \quad (2)$$

$$\delta = 100f \cdot D \quad (3)$$

the effective process conditions where the laser can work in PW mode results in a working area shown in Fig. 2.

Although this characteristic may appear as a limitation, compared to the modulated wave (MW) fibre sources with

equal pulse power or the pulsed Nd:YAG sources, the QCW offers several advantages, such as low investment cost, high wall-plug efficiency, reliability, zero maintenance, stability, a high-quality beam (the beam parameter product $BPP = \lambda M^2 / \pi$ equal to 2.4 mm × mrad, corresponding to a M^2 of about 2.2). The latter characteristic allows to obtain a very small beam diameter at the focussing point and is due to the possibility to use small diameter fibre (here 50 μm) regardless of the high pulse power. It is worth noting that the high wall-plug efficiency of the fibre laser is a great advantage when materials with low added value need to be machined since this permits a reduction of the overall product cost. As a matter of fact, the nominal power consumption of this laser source is only 1.8 kW; this value is a very low value when compared with the same power CO₂ or Nd:YAG source.

The laser system adopts a cutting head (IPG MICRO CUTTING HEAD P21-010,105 D25) with a nozzle of 0.8 mm in diameter, and a focusing lens of 100 mm in focal length. The latter allows obtaining a beam spot diameter (d_s) of about 80–100 μm. The CNC is controlled via a personal computer, allowing the cutting pattern generation and the process parameter setting such as the following: cutting speed, average power (P_a) in CW mode, and, in PW mode, the pulse power (P_p), the pulse duration (D), the pulse frequency (f), and the cutting speed (C_s).

2.3 Procedures

2.3.1 Composite fabrications and characterisation

Composite laminates with 500 mm × 400 mm in-plane dimensions and a thickness of 2.67 ± 0.16 mm, were

Fig. 2 Working area for the adopted laser source in terms of pulse duration and duty cycle vs. pulse power

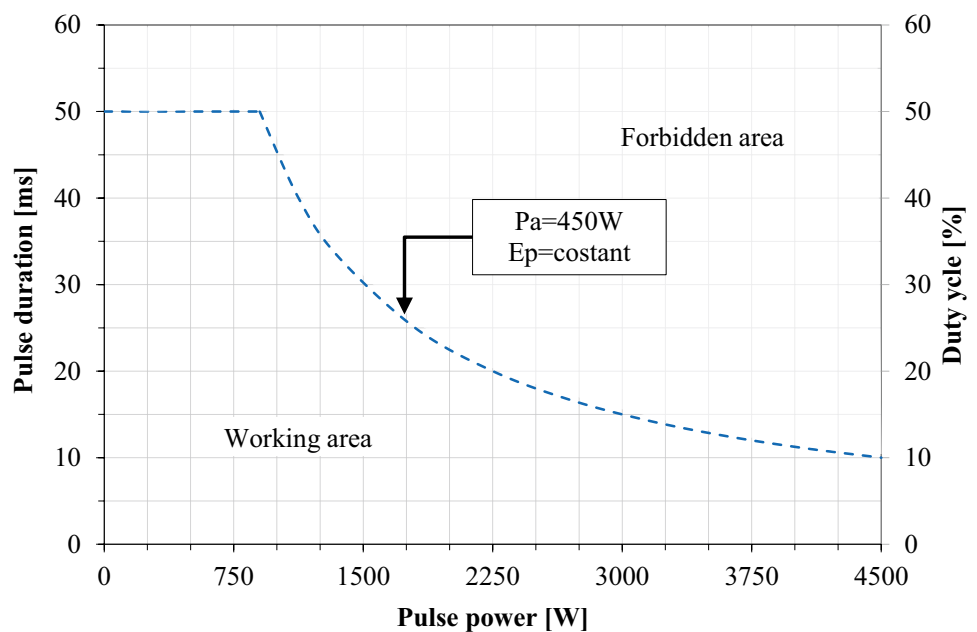
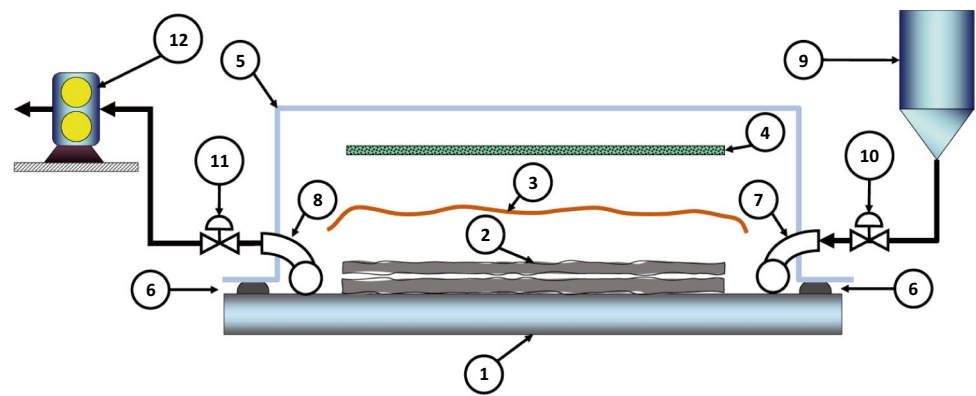


Fig. 3 Schematic of the infusion process setup

- | | | | | | |
|---|-------------------------|---|--------------------|----|--------------|
| 1 | Glass tool | 5 | Vacuum Bag | 9 | Resin tank |
| 2 | Non-woven carbon fabric | 6 | Vacuum sealant | 10 | Inlet valve |
| 3 | Peel-ply | 7 | Inlet distributor | 11 | Outlet valve |
| 4 | Distributor (net) | 8 | Outlet distributor | 12 | Vacuum pump |

obtained by means of the resin infusion process. To produce the required thickness, 2 plies of mat reinforcement were placed on a glass mould, previously treated with a release agent, and covered with a peel ply (nylon fabric) a polypropylene net, that acts as a distributor, and the plastic vacuum bag (polypropylene flexible bag). The latter was bonded to the glass tool with a butylic sealant (MATES® M-Seal) after the placement of the inlet and outlet distributor. A vacuum pump was adopted to realise the air suction. Once the vacuum (about -0.85 bar) was achieved, the resin system (SX8 EVO mixed with a low hardener) was sucked into the vacuum bag until the total impregnation is obtained. After that, the inlet valve was closed and the vacuum pump was left on for another hour to remove the matrix excess. Thus, the output valve was closed and the composite was left to consolidate for 24 h. After composite extraction, a post-cure process of 5 h at 70 °C was performed too. In Figs. 3

and 4, the schematic of the infusion process and images of the obtained laminate are reported, respectively.

Quasi-static tensile and 3-point flexural tests were carried out, according to the ASTM D 3039/D 3039 M-14 [74] and ASTM D 790–17 Standard specifications [75], respectively. The tests were performed adopting a universal testing machine (MTS ALLIANCE RT/50) equipped with a 50-kN load cell and, for the tensile tests, an extensometer 24 mm in length (MTS 634.31F–24). Due to the mat anisotropy [30], the tests were carried out in both the directions: longitudinal (L) and transversal (T) to the coil direction, highlighted in Fig. 4. The tests were carried out 1 week after the post-cure cycle; to assure the reproducibility of the results, five samples were tested for each test method and direction (L, T). In addition, ASTM D 792–20 [76] and ASTM D 3171–15 (Procedure G) [77] were adopted to measure the material density and the composite content, respectively. In

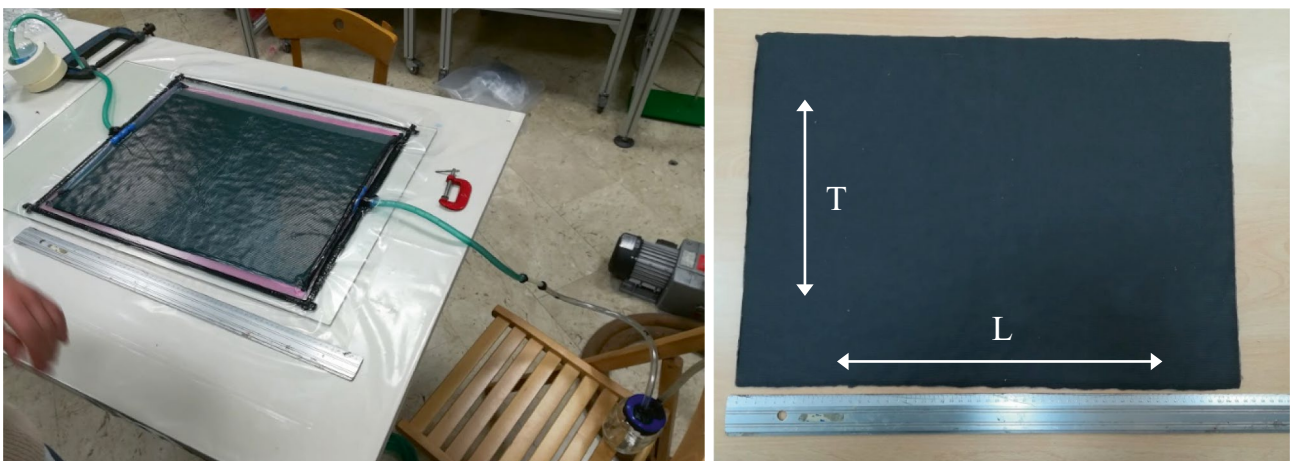
**Fig. 4** Images of the laminate during the fabrication and after de-moulding

Table 2, the measured mechanical properties (failure stress and Young's modulus) are reported. From the table, the mechanical properties are aligned to the ones measured in [30]; however, anisotropy is clearly visible. The latter is due to the partial alignment of the fibres along the coil longitudinal direction resulting from both the carding and the winding process phases. Considering the reinforcement format (non-woven carbon fabric), the reinforcement volume ratio, and the reinforcement cost (comparable to a glass fibre mat), the mechanical properties seem to be promising, since they are comparable or in some cases better to a glass fibre mat with the same resin content.

2.3.2 Laser cutting

The experimental plan was developed by adopting a systematic approach to the Design of Experiment (DoE) methodology. Compared to the typical approaches “one-factor-at-a-time”, the DoE approach has both the advantages of reducing the experimental runs and providing information about the effects of the interaction between the various process parameters [78, 79]. Typically, the DoE approach is not limited to the selection of the test plan (i.e. the factorial plan type), but it involves the selection of the control factors (i.e. the settable process parameters that affect the cutting process) and their levels, and the response variables (here the kerf geometry and the HAZ extension) as well as the knowledge and the bibliographic analysis.

The selection of the control factors (i.e. the settable process parameters that affect the cutting process) and the response variables (the measured quantity that describes the process behaviours) is a critical issue in statistical analysis, especially when several factors are affecting the process itself, like in laser cutting. In Fig. 5 the parameters affecting the kerf geometry and quality are reported as suggested by Mathew et al. in [50]. From the figure, the laser cutting process is affected by a large number of process parameters. However, since either the investigated material or the adoption of specific equipment imposes precise constraints (i.e. they are fixed), only a part of these

can be used as control factors; in Fig. 5 the possible control factors are highlighted by the italics bold text. Thus, the selection of the control factors and their levels were performed based on the relevant bibliography, previous experiences, and preliminary tests. More in detail compared to the CW mode, in PW mode it is possible to obtain significantly higher cutting speeds (an order of magnitude greater) and considering the industrial requirements (higher cutting speed = less cost), all the test campaign was carried out using the laser in pulsed regime; for the same reason, the average power was fixed at the maximum nominal value.

A further simplification can be made for the mode operation parameters (see Fig. 5) considering that in PW mode the settable parameters are P_p , D , and f . Thus, since the average power is fixed, only two of the above quantities can be selected independently, while the third must be derived by Eqs. (1)–(2). Thus, in the present case, the pulse power and the pulse duration were chosen as control factors, while the pulse frequency was selected, according to Eqs. (1)–(2), to satisfy the condition $Pa = 450$ W.

Then, P_p and D levels were selected based on previous experiences and preliminary tests, considering the process conditions allowing maximum cutting speed and minimum thermal damage.

Moreover, in PW mode, to avoid the cutting interruption, an appropriate value of the overlapping factor ($R\%$) is required (typically greater than 75%). The latter represents the superposition between two consecutive pulses (pulse overlapping) and can be calculated by the following expression:

$$R\% = \left[1 - \frac{(Cs/f)}{(df + Cs \cdot D)} \right] \cdot 100 \approx \left[1 - \frac{Cs}{f \cdot df} \right] \cdot 100 \quad (4)$$

where df is the beam footprint diameter or the beam spot diameter on the components (in this work the beam spot diameter was adopted). In Fig. 6 a representation of the overlapping factor is showed. From Eq. (4), by fixing the $R\%$ and f , the cutting speed (Cs) is fixed too as it is a derived quantity.

Table 2 Laminate properties according to the ASTM Standard

ASTM Standard	Test direction	Length (mm)	Width (mm)	Span (mm)	Thickness (mm)	Failure stress (MPa)	Young modulus (GPa)
D 3039-D 3039 M-14	L	250	21.5 ± 0.29	–	2.7 ± 0.22	203 ± 15.8	13.1 ± 0.69
	T	250	21.7 ± 0.14	–	2.7 ± 0.15	113 ± 9.2	8.7 ± 0.52
D790-17	L	200	13.5 ± 0.14	120	2.6 ± 0.14	245 ± 15.2	12.9 ± 1.16
	T	200	13.7 ± 0.7	120	2.6 ± 0.11	158 ± 9.8	8.1 ± 0.72
D 792–20	Density (kg/m ³)			1211 ± 7.42			
D3171-15, Procedure G	Reinforcement content (wt%)			12.62 ± 0.209			

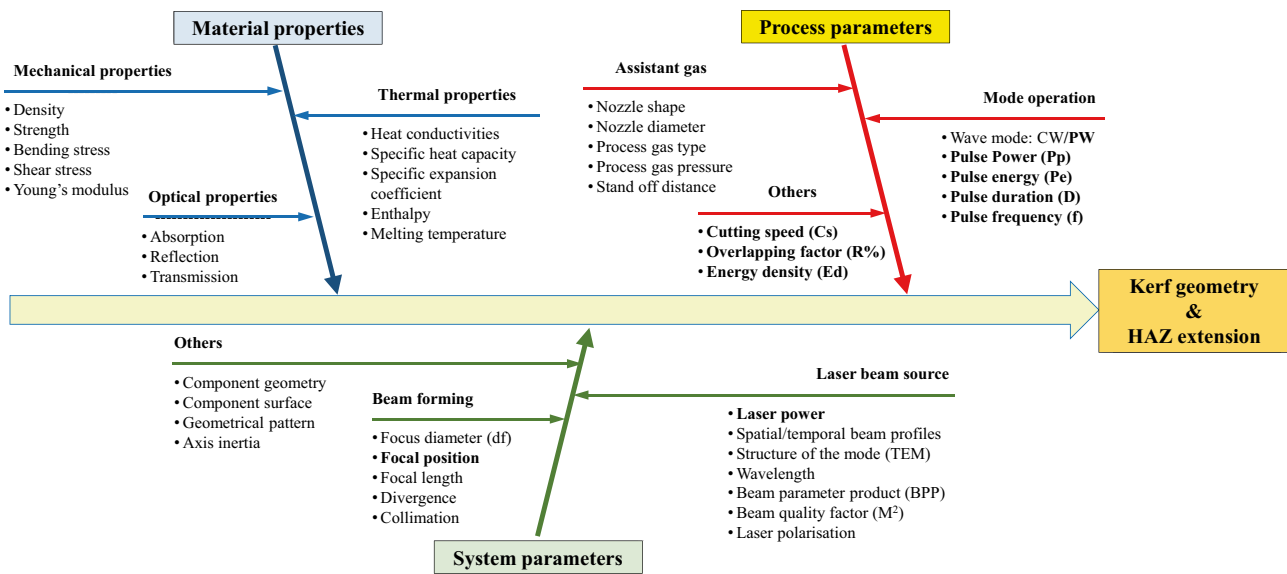


Fig. 5 Parameters affecting the kerf geometry and quality

The remaining parameters are the focal position, the nozzle diameter, the assist gas, and its pressure.

The former was selected on the component surface, considering the beam dimension at the component exit; the latter can be calculated by the following Eq. (5) [73]:

$$df_z = 2 \cdot w_z = w_0 \sqrt{1 + \left(\frac{\lambda \cdot z}{\pi \cdot w_0^2} \right)^2} \quad (5)$$

where w_0 is the radius at the focussing point (the beam waist), z is the distance from the focussing point, w_z is the radius at a distance z , and λ is the laser wavelength. Thus, for the adopted system at 2.7 mm (i.e. the laminate thickness) from the focussing point, the beam diameter is about 100–115 μm , which is still a sufficiently small value to allow

high power densities. The nozzle diameter was selected in the middle value of the available ones for the adopted cutting head (0.8), as assistant gas nitrogen at 7 bar (0.7 MPa) was adopted. The latter was selected at about 1/2 of the maximum pressure to avoid excessive kerf erosion. In addition, since the mechanical tests highlighted that the laminate shows a partial fibre alignment, during the plan development, the cutting directions with respect to the coil direction (longitudinal (L) or transversal (T)) were also considered control factors. This parameter was adopted since the direction of the fibres affects the heat diffusion within the matrix and then the HAZ extension [62]. Consequently, since the heat is transported along the fibres, it is expected that when the laser travels along the transverse direction (T), the thermal damage is greater than in the longitudinal one (L). In Table 3 the adopted control factors and their values are reported, while in Table 4, for completeness, the corresponding derived process conditions in terms of C_s and L_e are reported too. It is worth noting that the levels (values) adopted for the process parameters were selected based on previous experience [39, 40, 63, 64, 80] and after preliminary tests.

During the tests, each treatment (i.e. control factors combinations) was repeated two times (i.e. two replications) for each direction. Thus, a total of 81 experimental runs were executed. The trial order was block randomised (i.e. only the treatments for the same replication were randomised) to reduce the disturbance of any unconsidered noise factor.

The influence of the control factors on the response variables was assessed by the analysis of variance (ANOVA) and main effects plot analysis. The ANOVA tests the significant differences between the means of the response variables by partitioning its total variation into different sources (error,

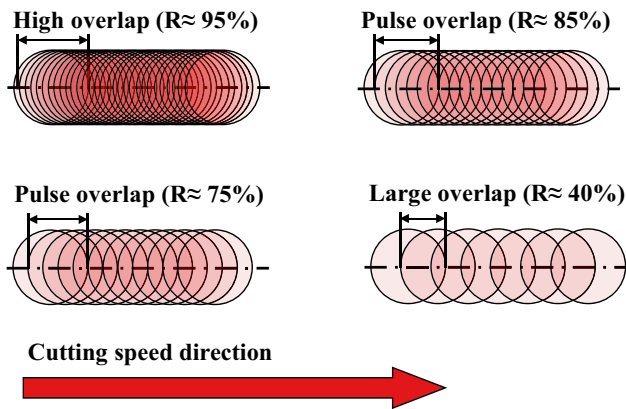


Fig. 6 Schematic of different pulse overlap percentages (R%)

Table 3 Control factors and levels adopted in the experimental plant

Control factor	Symbol	Unit	Levels		
			−1	0	+1
Direction	Dir		L	−	T
Pulse power	P_p	(kW)	3.00	3.75	4.50
Pulse duration	D	(ms)	0.05	0.15	0.25
Overlapping factor	R	(%)	75	80	85

experimental group membership...) and comparing the variance variability between groups (or treatments) with the one within the group (i.e. the same treatment). The analysis was performed with a confidence level of 95% ($\alpha=0.05$); thus, a control factor or an interaction is statistically significant if the p -value is less than 0.05. The F -value indicates the weight of the effect; the greater the F -value, the greater the variation of the response variables at control factors change.

The analysis was performed up to the second-order terms (i.e. considering only the main effect and the 2-way interactions, while the 3-way and the 4-way ones were not considered). From a practical point of view, this choice did not entail limitations to the analysis, except for a moderate lowering of the error estimators (R-sq and R-sq(adj)).

2.3.3 Kerf characterisation

After the tests, the samples were cut by a diamond saw, embedded with white acrylic paint, and polished using abrasive paper of grit size up to P2500 (Standard ISO 6344). The response variables considered for this study are the kerf widths at the entrance of the beam (upper side) and the output one (bottom side); the matrix recession (MR, i.e. the extension of the kerf wall where the fibres protrude from the matrix); and the HAZ extension. The latter is the width of the overall damage extension of the matrix that comprises the MR and the matrix degradation. The kerf geometry characterisation was performed according to the UNI EN ISO 12584 and ISO 9013 in the section. In addition, as suggested by several authors [81–83],

measurements on the external surfaces (upper and bottom) were carried out too. In Table 5 the adopted response variables are summarised, while in Fig. 7 the schematic of how they were measured is reported. For the HAZ measured in the section, during the analysis the average value between the two sides (left and right) was adopted, as proposed by Tagliaferri [84] and Jovane [85]. Since it is possible to take more images on the same external surfaces, the measures on the surfaces were repeated three times, and the average values were adopted in the analysis. In addition, the taper angle was calculated from the kerf widths measured in the section (Ta_S) and on the external surfaces (Ta) according to the following equations:

$$Ta_S = \tan^{-1}[(Uk_S - Bk_S)/(2 * t)] \quad (6)$$

$$Ta = \tan^{-1}[(Uk - Bk)/(2 * t)] \quad (7)$$

where t is the nominal thickness (2.7 mm). Moreover, since the measurement carried out on the external surfaces is acquired in different positions, in Eq. (7), the Ta was evaluated adopting the average value of the three measures of Uk and Bk performed on each sample.

3 Results and discussion

3.1 Optical analysis

Figures 8, 9, 10, and 11 show the beam entrance surface, the kerf section, and the surface for cuts obtained in different conditions along with both the directions (Figs. 8 and 9 along the transversal direction (T); Figs. 10 and 11 along the longitudinal direction). From the figures, the upper kerf width always appears less or equal to the bottom one. Therefore, the taper angles fall in the negative region (i.e. $<0^\circ$). In addition, the upper kerf shows little variation with process parameters, while Bk increases by increasing the pulse duration and R . The thermal damage mainly consists of fibre pull out and matrix recession. A

Table 4 Calculated C_s (mm/min) and Le [J/mm] for the adopted process conditions (P_p , D , and R)

P_p (kW)	$D=0.05$ (ms)			$D=0.15$ (ms)			$D=0.25$ (ms)		
	$R=75\%$	$R=80\%$	$R=85\%$	$R=75\%$	$R=80\%$	$R=85\%$	$R=75\%$	$R=80\%$	$R=85\%$
3.00	2700 (10)	2160 (13)	1620 (17)	900 (30)	720 (38)	540 (50)	540 (50)	432 (63)	324 (83)
3.75	2160 (13)	1728 (16)	1296 (21)	720 (38)	576 (47)	432 (63)	432 (63)	346 (78)	259 (104)
4.50	1800 (15)	1440 (19)	1080 (25)	600 (45)	480 (56)	360 (75)	360 (75)	288 (94)	216 (125)

All the process conditions correspond to a fixed average power of 450 W
In the round brackets are indicated the Le values

Table 5 Adopted response variables and their nomenclature

Measuring position		Response variables	Symbol	Unit
External surfaces	Upper	Kerf width	Uk	(μm)
		Max matrix recession	MR_U	(μm)
		Max HAZ extension	HAZ_UM	(μm)
	Bottom	Kerf width	Bk	(μm)
		Max matrix recession	MR_B	(μm)
		Max HAZ extension	HAZ_BM	(μm)
Section	Upper kerf width		Uk_S	(μm)
	Bottom kerf width		Bk_S	(μm)
	HAZ measured at 10% of the thickness from the upper surface		HAZ_SU	(μm)
	HAZ measured at 10% of the thickness from the bottom surface		HAZ_SB	(μm)
	Max HAZ		HAZ_SM	(μm)
	Taper angle*		Ta_S	(Deg)

*Calculated through Eqs. (6) and (7)

limited number of delaminations were observed (Figs. 8d and 9b–d). However, it was possible to observe that the delamination occurs only in correspondence with porosity. The width of the matrix recession seems to increase with increasing the pulse duration and pulse power and the overlapping factor, while, as expected, it is lower when the laser beam works along the longitudinal direction (L), as visible comparing Figs. 8 and 9 to Figs. 10 and 11.

Moreover, for the cutting condition corresponding to the simultaneous combination of the lower values of P_p , D , and R , the through cut is interrupted (Figs. 8a and 10a). It is worth noting that during the preliminary tests, all cuts were through; thus, this condition corresponds to the limit beyond which it is not possible to carry out the through cut ($P_p = 3 \text{ kW}$, $D = 0.05 \text{ ms}$, $R = 75\%$, and $C_s = 2700 \text{ mm/min}$). Consequently, the statistical analysis (described in the

Fig. 7 Schematic of the adopted response variables (kerf geometry and HAZ extension) measured on **a–b** kerf section; **c–d** external surfaces

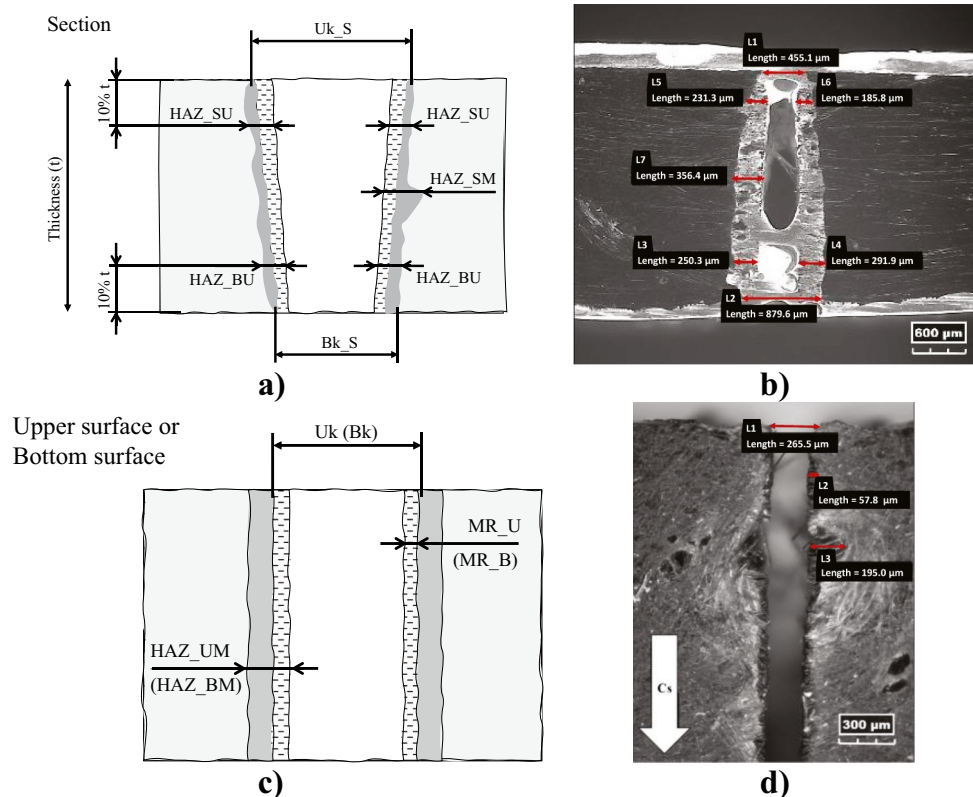
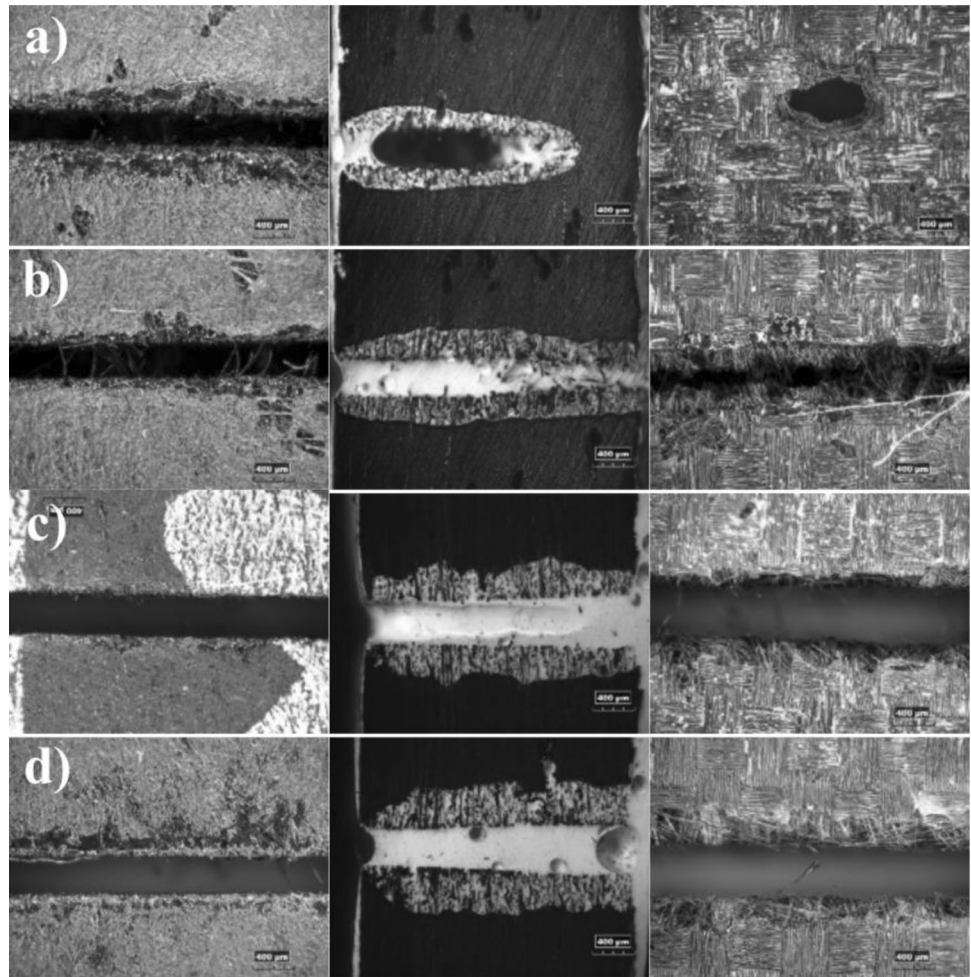


Fig. 8 Images of upper, section, and bottom kerf obtained cutting along the transversal direction (T) at $P_p = 3$ kW, and **a** $D = 0.05$ ms, $R = 75\%$; **b** $D = 0.05$ ms, $R = 85\%$; **c** $D = 0.25$ ms, $R = 75\%$; **d** $D = 0.25$ ms, $R = 85\%$. In the sections, the upper surfaces are on the left



following paragraph) was performed after deleting the data measured in the bottom part of the kerf in correspondence to these process conditions (i.e. the analysis is unbalanced).

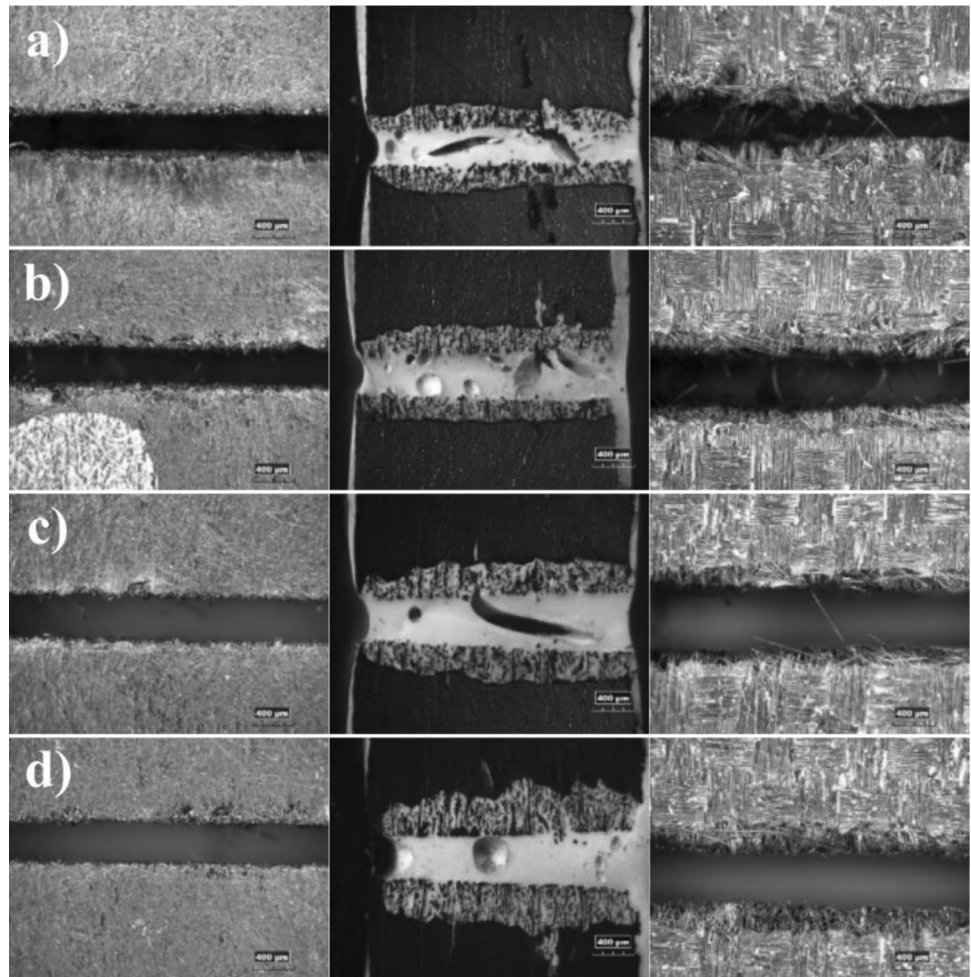
3.2 ANOVA results

Before the analysis, the ANOVA assumptions were verified by the graphical examination of residuals, according to what was reported in [78]. In only one case (the matrix recession measured on the bottom surface, MR_B), problems with the residual's normal distribution were observed. For this parameter, the Cox-Box transformation was successfully adopted. However, for the sake of brevity, this part of the analysis was not described here. In Tables 6 and 7, the results of the ANOVA are summarised for all the measurable response variables in terms of p -value and F -value, for the measurements carried out in the sections and on the surfaces, respectively, while in Table 8 the ANOVA results for Ta_S and Ta are reported (that are calculated variables). Since the analysis was carried out adopting a 95% confidence level, a control factor is statistically significant if the p -value is less than 0.05. Similarly,

a p -value < 0.05 for the two-factor interaction indicates that the effect of a control factor on the response variables depends on the adopted level of another control factor. In the tables, the significant control factors are highlighted by bold text. F -value indicates the weight of the effect: the greater the F -value, the greater the variation of the response variables at control factor changes. The tables also provide the error estimators: R-sq [%] and R-sq(adj) [%]. R-sq [%] describes the amount of the response variable variation explained by the control factors, while the R-sq(adj) [%] is a modified R-sq that has been adjusted for the number of terms in the model.

From the tables, the fibre direction (T/L) affects the upper kerf width measured on the external surface and the HAZ parameters measured in both the section and on the external surfaces; the P_p affects the Bk_S, the HAZ_SM, and the HAZ_BM; the pulse duration (D) affects all the response variables except the upper kerf (UK_S and UK), while the overlapping factor does not affect the upper kerfs and the HAZ_BM. Comparing the F -values, the most affecting control factor is the pulse duration which shows an F -value one order of magnitude higher than the other factors.

Fig. 9 Images of upper, section, and bottom kerf obtained cutting along the transversal direction (T) at $P_p = 4.5$ kW, and **a** $D = 0.05$ ms, $R = 75\%$; **b** $D = 0.05$ ms, $R = 85\%$; **c** $D = 0.25$ ms, $R = 75\%$; **d** $D = 0.25$ ms, $R = 85\%$. In the sections, the upper surfaces are on the left



Moreover, the tables also show several significant interactions. However, compared to the main factors, their F -values are low and no anti-synergic interactions were recorded. Therefore, in the following analysis, they have been neglected.

3.3 Effect of process parameters and interaction mechanisms

In Figs. 12, 13 and 14 the main effect plots of the response variables for the section, surface, and derivate quantities (taper angles) are reported. In the figures, the significant parameters are highlighted by a continuous line. From the figures, it is notable that the upper kerf (UK) increases when the laser cuts along the longitudinal direction (Fig. 13a). However, in this case, it must be considered that the R -sq is very low (Table 7: R -sq = 37.70); consequently, the variation indicated by the control factor is also low which indicates that the response variable is scarcely affected by the analysed parameter.

The bottom kerf widths increase at the increase of D , R , and P_p (Figs. 12b and 13b) indicated in the order of

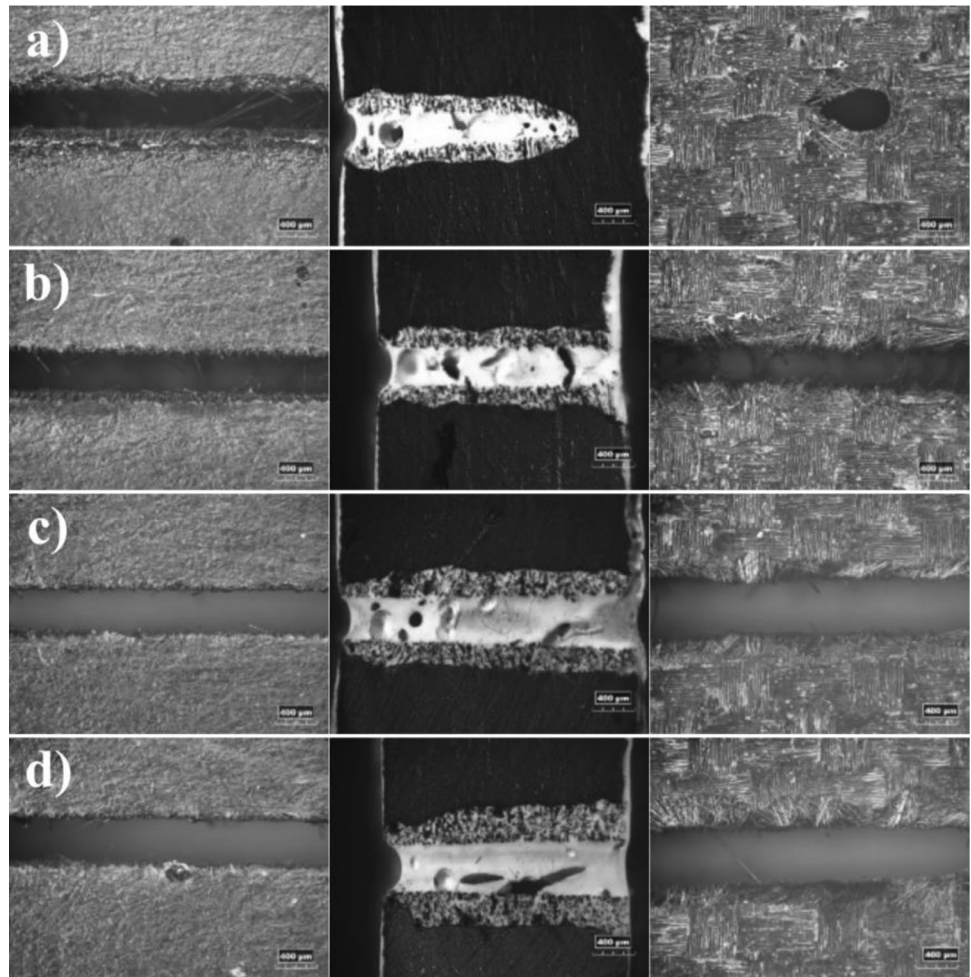
importance (i.e. with higher F -value). The HAZs measured in the section show similar behaviour (Fig. 12c–e); they increase at the increase of D and R or passing from the longitudinal (L) to the transversal (T) direction; moreover, HAZ_SM (Fig. 12e) also increases as P_p increases.

MR_U and MR_B show opposite behaviours (Fig. 13c–d): the latter increases at the increase of D and R or passing from the L to the T direction, and vice versa for the MR_U. Furthermore, the matrix recession extension is always greater on the lower surface (approximately double for almost all the analysed process conditions).

Compared to the HAZs measured in the sections, the HAZs measured on the surfaces (HAZ_UM and HAZ_BM, (Fig. 13e–f)) show an opposite effect since they decrease at the increase of the pulse duration (D); moreover, HAZ_UM decreases at the R increases, while HAZ_UB decreases at the P_p increase. However, according to the HAZ measured in the section, both HAZ_UM and HAZ_BM increase passing from the longitudinal to the transversal direction.

Lastly, since the upper kerfs are scarcely affected by the process parameters, the taper angles (both Ta_S and Ta) follow, according to the Eqs. (6)–(7), an opposite

Fig. 10 Images of upper, section, and bottom kerf obtained cutting along the longitudinal direction (L) at $P_p = 3$ kW, and **a** $D = 0.05$ ms, $R = 75\%$; **b** $D = 0.05$ ms, $R = 85\%$; **c** $D = 0.25$ ms, $R = 75\%$; **d** $D = 0.25$ ms, $R = 85\%$. In the sections, the upper surfaces are on the left



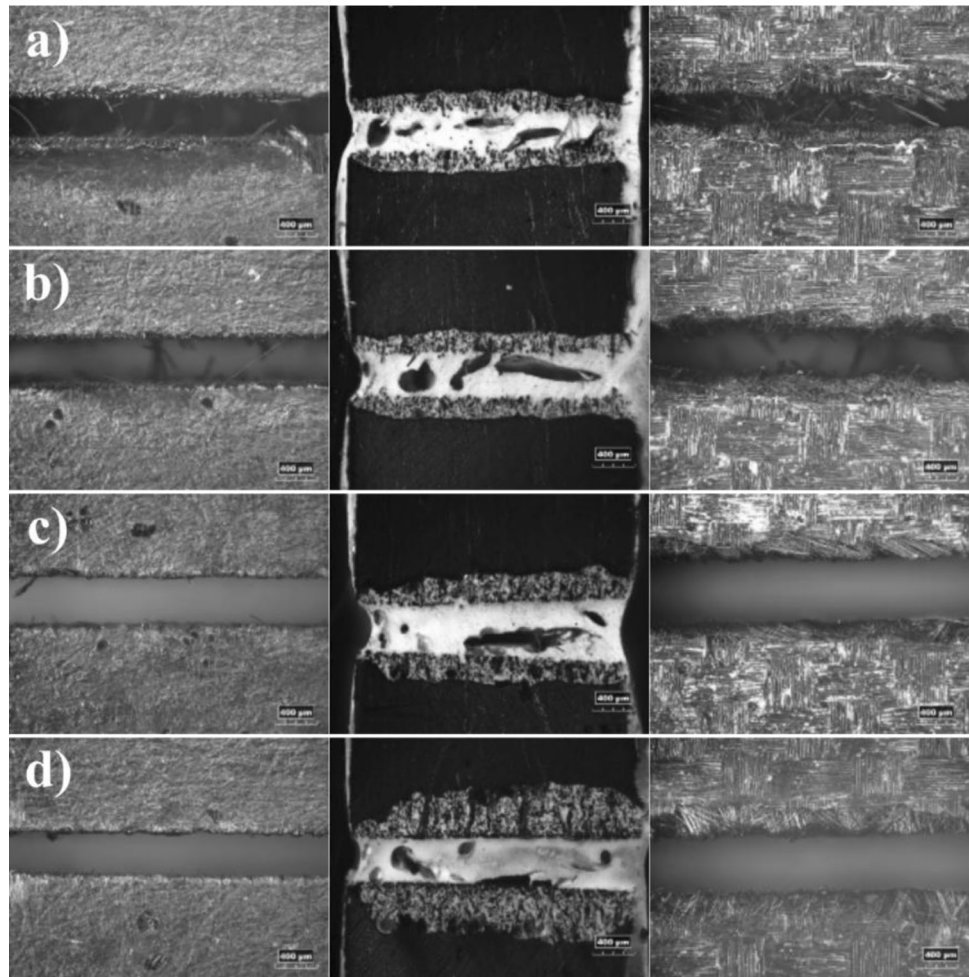
trend compared to the bottom kerf width: when the latter increases, the former decreases.

Combining the comments and the observation of Figs. 8 and 12, the following interaction mechanisms can be deduced: the laser beam directly impacts the upper surface; on this surface, the beam is absorbed by the fibres that rapidly vaporise producing a great quantity of vapours at high pressure. Simultaneously the matrix around the fibres absorbs the heat from the fibres and vaporises forming further gases. The gases completely absorb the laser radiation and transfer the energy to the sidewalls of the kerf both by convection and by radiation. In this area, the fibres are not directly exposed to the radiation and remain partially intact; this justifies the presence of the central channel with a quasi-constant cross-section without fibres. However, since the fibres have high thermal conductivity, they conduct a further quantity of heat to the surrounding matrix. The presence of the three heat transfer mechanisms causes a matrix burnout on the surrounding walls, producing a strong flame, clearly visible during the cutting operation. The flame intensity depends on the process parameters; in any case, it is mainly oriented downwards and in the opposite direction concerning the direction of the laser beam.

The effects of D and R on the HAZs measured in the section and the kerf width can be explained considering that an increase in the duration or the overlapping factor (that is an inverse function of the linear energy) involves an increase in the interaction time; the latter allows the introduction of a higher quantity of heat that causes an enlargement of the kerf and the increase of the HAZ.

Moreover, the presence of the assistant gas (at 7 bar) on the upper kerf region causes the cooling of the upper surface and the concentration of the plasma action and the heat in the bottom kerf area, making the measured at the bottom (BK, BK, HAZ_SB, and HAZ_SM) more sensitive to the process conditions. At the same time, this explains the scarce effect of the process parameters on the upper kerfs. The effect of the travel beam direction is a consequence of the partial fibre alignment: since there are more fibres aligned to the longitudinal direction, the thermal conductivity is higher along the latter. Then, when the laser beam travels in the transverse direction, the amount of heat transmitted by conduction to the sidewalls of the kerf tends to increase and therefore an increase in both the kerf width and the HAZ extension occurs.

Fig. 11 Images of upper, section, and bottom kerf obtained cutting along the longitudinal direction (L) at $P_p = 4.5$ kW, and **a** $D = 0.05$ ms, $R = 75\%$; **b** $D = 0.05$ ms, $R = 85\%$; **c** $D = 0.25$ ms, $R = 75\%$; **d** $D = 0.25$ ms, $R = 85\%$. In the sections, the upper surfaces are on the left



The pressure of the assistant gas also causes the erosion of the fibres protruding from the matrix and the burned matrix presents on the upper surface. This effect is stronger when the fibres are partially aligned along the laser beam

direction since along this direction the length of the exposed fibres is higher. This explains both the increases of UK and MR_U when the laser beam travels along the longitudinal direction.

Table 6 ANOVA table for the response variables measured in the section

Source	Uk_S (μm)		HAZ_SU (μm)		Bk_S (μm)		HAZ_SU (μm)		HAZ_SM	
	F-value	p-value	F-value	p-value	F-value	p-value	F-value	p-value	F-value	p-value
Direction	0.81	0.370	22.41	0.000	2.16	0.146	65.78	0.000	34.11	0.000
P_p (kW)	0.97	0.384	1.68	0.193	6.30	0.003	3.13	0.050	3.20	0.046
D (ms)	0.21	0.810	15.40	0.000	122.80	0.000	151.56	0.000	87.50	0.000
R (%)	0.55	0.578	7.52	0.001	23.30	0.000	56.57	0.000	33.44	0.000
Direction $\times P_p$	0.31	0.734	3.22	0.045	1.37	0.259	1.27	0.288	0.07	0.931
Direction $\times D$	1.31	0.276	5.07	0.008	0.69	0.507	4.45	0.015	3.74	0.028
Direction $\times R$	0.49	0.613	0.87	0.423	0.33	0.718	2.02	0.139	1.03	0.363
$P_p \times D$	0.17	0.955	0.72	0.579	3.54	0.011	0.79	0.534	0.47	0.760
$P_p \times R$	0.32	0.866	1.31	0.275	1.38	0.247	0.12	0.974	0.28	0.887
$D \times R$	0.79	0.536	1.54	0.200	3.78	0.007	10.54	0.000	9.25	0.000
R-sq (%)		14.77		55.13		80.31		88.76		79.81
R-sq(adj) (%)		0.00		41.11		73.75		84.97		73.50

Table 7 ANOVA table for the response variables measured on the surfaces

Source	Upper surface						Bottom surface					
	Uk (μm)		Mr_U (μm)		HAZ_UM (μm)		Bk (μm)		Mr_B (μm)		HAZ_BM (μm)	
	F-value	p-value	F-value	p-value	F-value	p-value	F-value	p-value	F-value	p-value	F-value	p-value
Direction	28.85	0.000	18.61	0.000	8.82	0.004	0.46	0.499	10.52	0.002	16.78	0.000
P_p (kW)	0.04	0.964	2.49	0.089	1.02	0.366	14.63	0.000	0.86	0.428	8.99	0.000
D (ms)	2.45	0.093	89.41	0.000	83.89	0.000	191.46	0.000	17.11	0.000	15.20	0.000
R (%)	3.23	0.045	14.68	0.000	5.07	0.008	27.70	0.000	21.96	0.000	1.56	0.216
Direction $\times P_p$	0.37	0.694	0.05	0.954	0.49	0.617	0.64	0.532	1.43	0.245	0.50	0.612
Direction $\times D$	0.33	0.723	4.89	0.010	5.12	0.008	0.22	0.803	0.08	0.925	0.54	0.584
Direction $\times R$	0.01	0.990	1.65	0.198	2.33	0.104	0.59	0.559	0.15	0.864	0.21	0.810
$P_p \times D$	0.73	0.572	3.06	0.021	1.98	0.106	4.95	0.001	0.50	0.733	1.05	0.390
$P_p \times R$	0.61	0.653	1.37	0.251	2.81	0.031	1.83	0.132	0.76	0.556	0.72	0.582
$D \times R$	0.63	0.640	7.68	0.000	3.10	0.020	5.64	0.001	2.58	0.044	6.06	0.000
R-sq (%)	37.70		78.16		74.23		86.66		61.45		56.44	
R-sq(adj) (%)	18.71		71.50		66.37		82.10		48.43		41.72	

On the other hand, the low reinforce percentage, the fibre random distribution (even if prevalent with respect to one direction), and the absence of dense (thick) tows capable of creating preferential paths for heat diffusion, make the heat transmission more homogeneously distributed on the surface of the kerf wall. Therefore, delaminations due to heat concentration along the tows are avoided.

It is worth noting that the main interaction mechanisms are consistent with those reported in the main bibliography for the traditional laminate [35, 50–52, 62–64], as well as the ones observed in laser cutting of a traditional laminate 1.3 mm in thickness, in the same process conditions [80].

Moreover, comparing the results obtained in this work to the one reported in [80], the main differences concern the kerf shape, HAZ extension, and delaminations. Respectively, the shape appears more regular (vertical) rather than barrel; the HAZ extension, despite the difference in thickness, is lower for the recycled fibre composite; the delaminations are absent with the same cutting speed despite the thickness being double. Based on the last affirmations, it is confirmed that, compared to the traditional laminates, the material investigated in this paper shows better workability.

3.4 Damage index individuation and optimal process condition

In Fig. 15 the response variable distributions are compared for homogeneous quantities (i.e. geometrical and HAZ extension). The quantities measured in the sections show mean values and standard deviations that are always greater than the reciprocal quantities measured on the surfaces; therefore, the measurements performed on the surface underestimate the quantities and vice versa. In addition, as already observed, the measurements made on the upper surfaces are lower in value than those recorded on the bottom ones and are affected by local phenomena (for instance the effect of the abrasion action due to the assistant gas).

To highlight the presence of relations between the different control factors, a correlation analysis was performed. Since the measurements in the section and the ones acquired on the surfaces were carried out at different points, the analyses were performed adopting the average

Table 8 ANOVA table for the taper angle

Source	Ta_S (deg)		Ta (deg)	
	F-value	p-value	F-value	p-value
Direction	1.13	0.292	15.69	0.000
P_p (kW)	4.41	0.015	12.59	0.000
D (ms)	80.39	0.000	184.47	0.000
R (%)	18.62	0.000	34.07	0.000
Direction $\times P_p$	2.99	0.056	0.89	0.413
Direction $\times D$	3.05	0.053	0.52	0.600
Direction $\times R$	0.06	0.946	0.50	0.609
$P_p \times D$	2.66	0.039	4.71	0.002
$P_p \times R$	0.78	0.542	1.27	0.289
$D \times R$	1.56	0.193	4.82	0.002
R-sq (%)	74.90		86.41	
R-sq(adj) (%)	66.64		81.75	

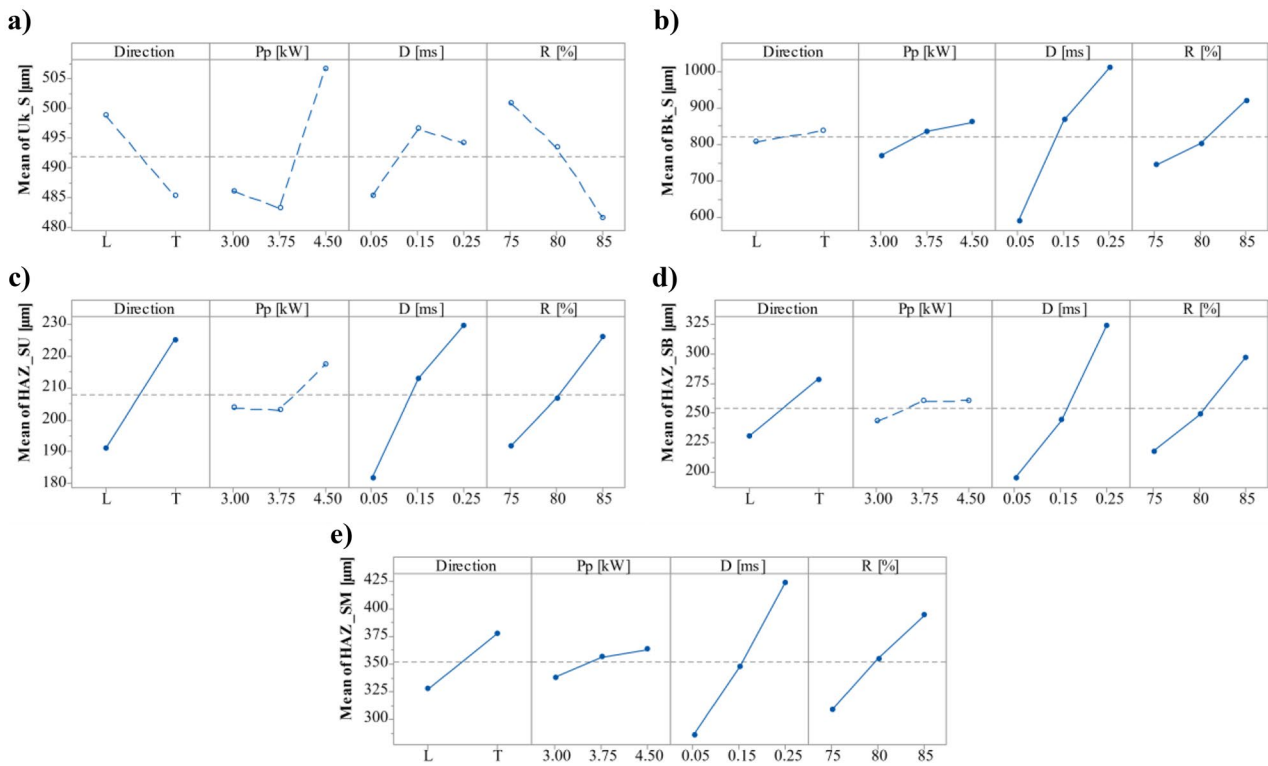


Fig. 12 Main effect diagrams for the measurements carried out in the kerf sections

value of the two replications. In addition, the correlation was performed by comparing homogeneous quantities and adopting a linear model. In Tables 9 and 10 the results of

the correlation analysis are reported for the geometrical and the damage response variables, respectively. In the tables the following codes were adopted:

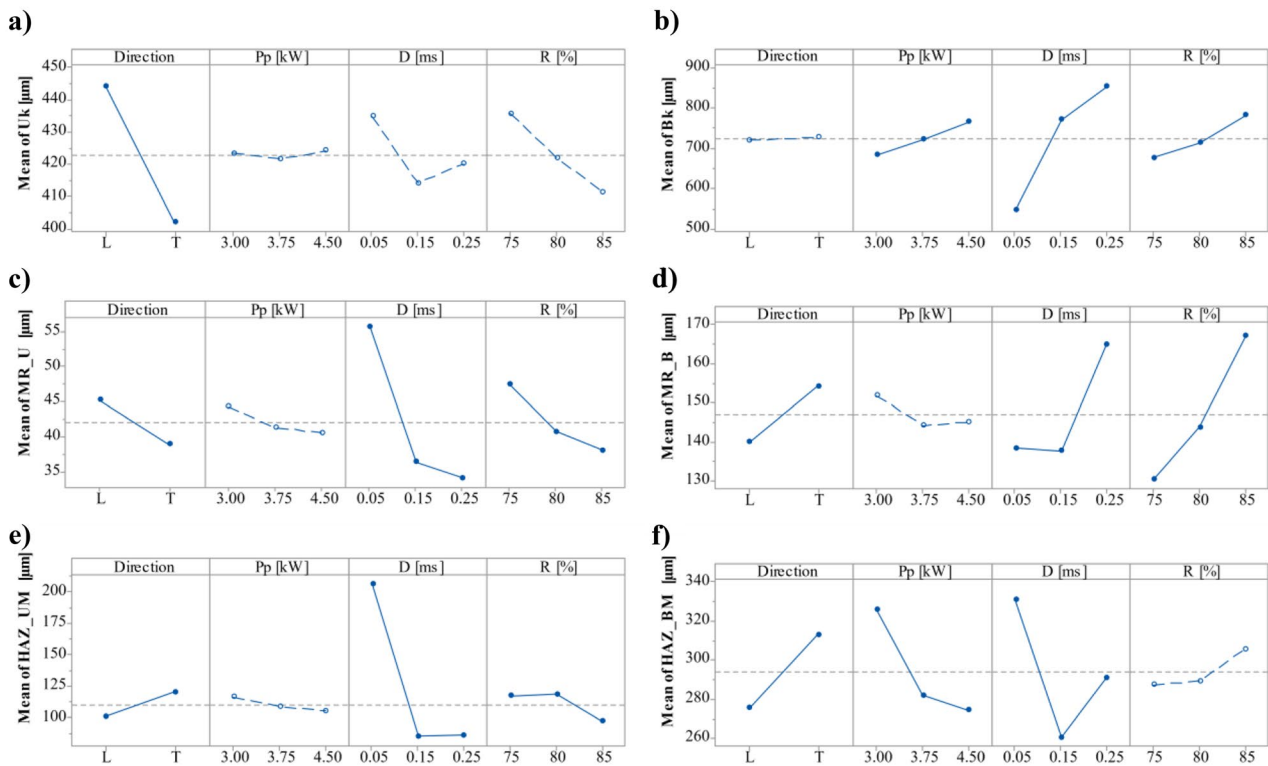


Fig. 13 Main effect diagrams for the measurements carried out on the kerf

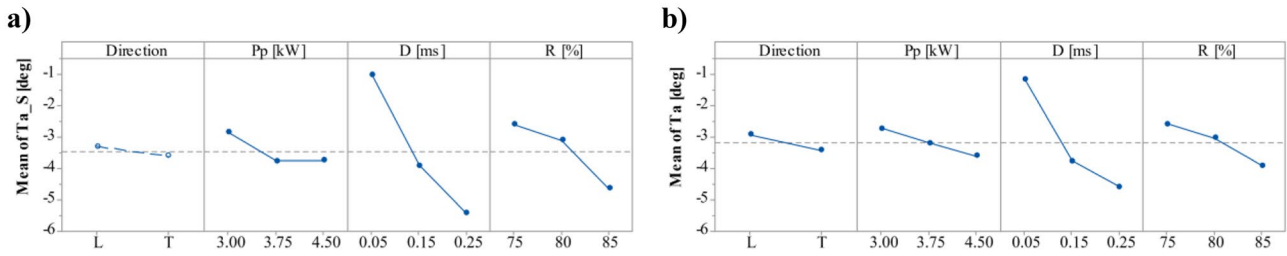


Fig. 14 Main effect diagrams for the taper angle

- ns, not significant: it means that no correlation (p -value > 0.05) was found;
- s, significant: it means that a correlation was found (p -value > 0.05) but the R_{sq} is less than 70%;
- numerical value: it indicates directly the R_{sq} value for correlation that have p -value > 0.05 and R_{sq} > 70%.

From the tables, no strong correlations between the variables measured at the surfaces and in the section are observed, except for the kerf widths and the HAZs measured at the bottom kerf. About the taper angles, the lack

of sensitivity to the process parameters of the upper kerf widths explains the strong correlation with the bottom kerf widths, as aforementioned. These results are consistent with previous work [80].

Although the measurements carried out on the surfaces are faster since they do not require sample preparation, and it is also possible to read more values on the same surface, those measurements could be affected by different noise factors. Firstly, compared to the images acquired in the sections, the surface ones are affected by a lower contrast; thus, there are more possibilities of errors in the measuring itself. Secondly, the measurements are subjective and depend on the operator’s skill; consequently, different operators can

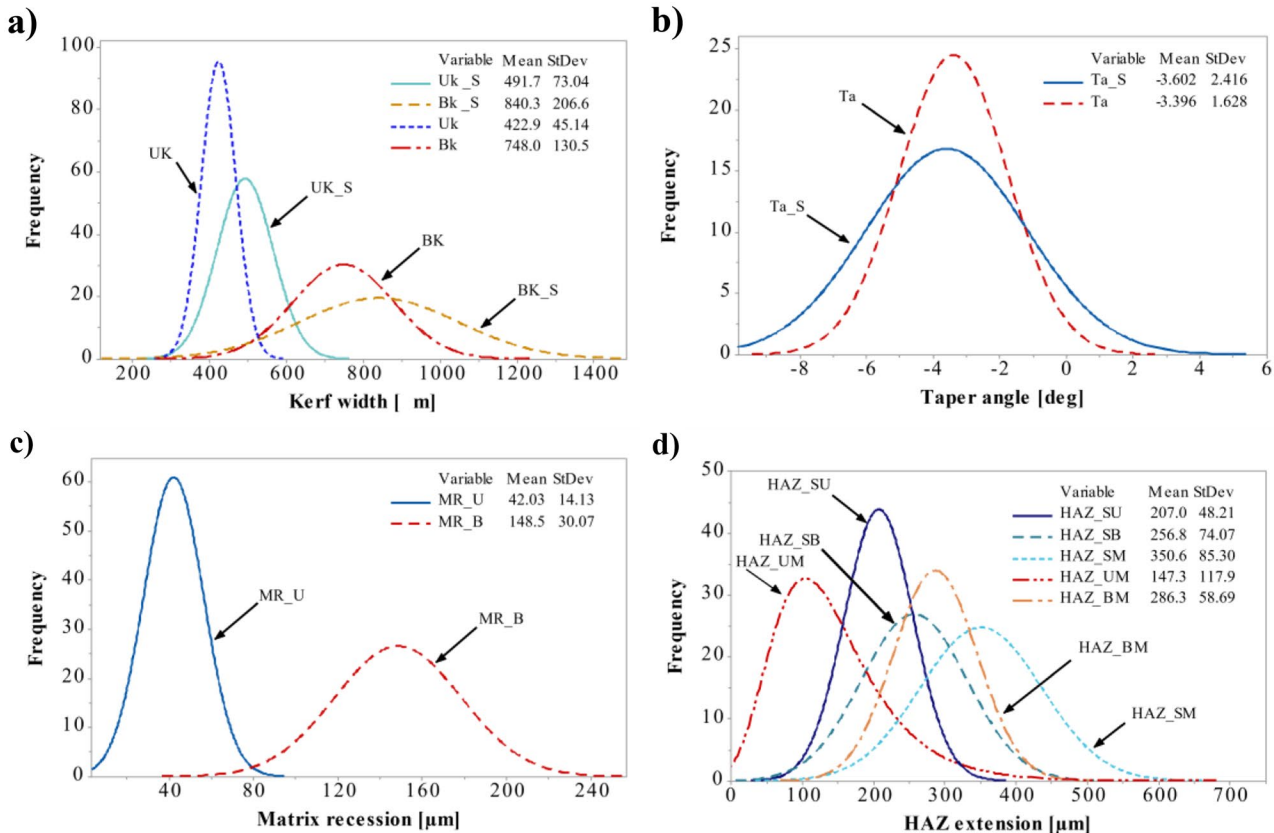


Fig. 15 Response variable distributions: a kerf widths; b taper angles; c matrix recessions; d HAZ extensions

Table 9 Results of correlation analysis for the geometrical response variable

	Uk	Bk	Ta	Uk_S	Bk_S	Ta_S
Uk	100	s	s	ns	s	ns
Bk	s	100	94.05	ns	93.89	92.27
TA	s	94.05	100	ns	86.31	92.37
Uk_S	ns	ns	ns	100	ns	ns
Bk_S	s	93.89	86.31	ns	100	96.66
TA_S	ns	92.27	92.37	ns	96.66	100

ns, non-significative: p -value > 0.05 or R-sq [%] $< 70\%$
 s, significative: p -value < 0.05 and R-sq [%] $< 70\%$
 Numerical value = R-sq [%], p -value < 0.05 and R-sq [%] $> 70\%$

Table 10 Results of correlation analysis for the damage response variable

	MR_U	HAZ_UM	MR_B	HAZ_BM	HAZ_SU	HAZ_SB	HAZ_SM
MR_U	100	89.54	s	s	s	s	s
HAZ_UM	89.54	100	ns	s	s	s	s
MR_B	s	ns	100	s	s	s	s
HAZ_BM	s	s	s	100	ns	ns	ns
HAZ_SU	s	s	s	ns	100	s	s
HAZ_SB	s	s	s	ns	s	100	93.53
HAZ_SM	s	s	s	ns	s	93.53	100

ns, non-significative: p -value > 0.05 or R-sq [%] $< 70\%$
 s, significative: p -value < 0.05 and R-sq [%] $< 70\%$
 Numerical value, R-sq [%], p -value < 0.05 and R-sq [%] $> 70\%$

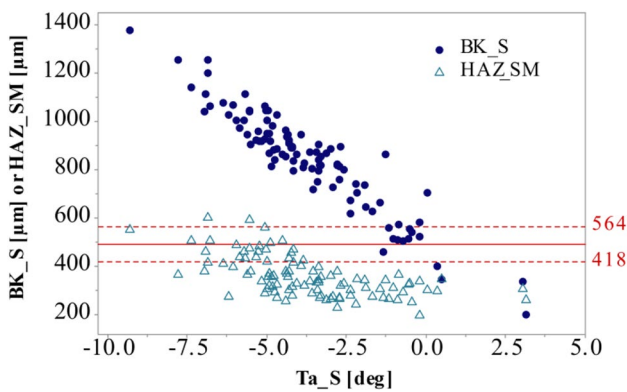


Fig. 16 Bottom kerf width and HAZ maximum measured in the section as a function of the taper angle. In the figure, the horizontal lines indicate the average value of the UK_S (continuous line) and its standard deviation (dashed lines)

measure different quantities. Moreover, large damages produced inside the kerf can be hidden by the front layers; therefore, they are not recorded during the analysis of the surface. Conversely, the section images appear well defined and contrasted. The damage produced in the inner part of the kerf is clearly visible, which indicates a more accurate measure since it is less sensitive to the operator’s skill; besides, the HAZ measured in the section is not underestimated.

Considering what was stated aforementioned about Fig. 15 and the scarce influence of the process parameters on the upper kerf widths, assuming a conservative approach (high damage = lower error), the use of the Bk_S, HAZ_SM, and Ta_S appears the appropriate choice to define one or more quality indexes and optimal process conditions. In Fig. 16, by plotting the BK_S and the HAZ_SM as a function of the taper angle Ta_S, it is possible to observe that a narrow area, characterised by a low HAZ (about 300 μm) and a taper angle close to 0°, is present. This area corresponds to the process conditions: $P_p = 3$ kW, $D = 0.05$ ms, and $R = 80\%$ ($C_s = 2160$ [mm/min]), which represents the optimal process condition.

4 Conclusions

In the present work, a 450-W QCW laser source was adopted to cut CFRP produced by adopting recycled carbon fibres. During the tests, the laser beam travel direction, the pulse power, the pulse duration, and the overlapping factor were changed. The kerf width and the HAZ extension were measured at the upper and bottom sides of the kerf, in the section, and on the external surface. ANOVA was adopted to assess the process parameter influence. From the results, within the adopted source,

material, and process conditions, the following main conclusions were drawn:

- The 450/4500 QCW fibre laser, despite the limited average power (450 W), can cut CFRP plates with recycled carbon fibres of 2.7 mm in thickness, at a maximum cutting speed of about 2000 mm/s.
- The interaction mechanisms observed for the composite obtained by adopting recycled fibres are similar to the ones described in the main bibliography for traditional laminate. However, the partially random distribution of the fibres and the absence of dense tows, which improve the heat flow in the surrounding matrix, allow a more regular kerf profile and lower HAZ (matrix degradation and fibre pull-out) and avoid large delaminations.
- The kerf width and the HAZ measured at the laser beam input side are scarcely influenced by the process parameters. The kerf width and the HAZ measured on the laser beam exit side are more sensitive to the investigated parameters. The most affecting process parameter is the pulse duration (D) since, regardless of the measured parameters and position, its F -value is one order of magnitude higher than the other, followed by the pulse overlapping (R) and the pulse power (P_p).
- The cutting direction mainly affects the extension of the HAZ. However, this is a consequence of the partial fibre alignment, which involves a moderate anisotropy in the thermal properties.
- To reduce the HAZ as much as possible, low values of P_p , D , and R are required. The latter corresponds to the adoption of the maximum cutting speed and then the maximum productivity. Here, the minimum HAZ extension ($HAZ_S \approx 300 \mu\text{m}$) was found for $P_p = 3 \text{ kW}$, $D = 0.05 \text{ ms}$, $R = 80\%$. In this condition, a taper angle of about 0° is also obtained.
- The correlations between the measurements performed in the section and on external surfaces were studied too. Results show that a correlation can be found only for the measures carried out at the bottom kerf. The measurements carried out in the section, despite being time expensive, appear to be more reliable and conservative compared to the surface ones.
- Finally, since for these materials another key to success is the possibility to adopt low-cost and high-productivity manufacturing processes, and it was proven that the material can be easily machined with a QCW laser source, the adopted material is very attractive for industrial applications.

Acknowledgements The authors are particularly grateful to the Interuniversity Research Centre CIRTIBS for providing part of the equipment to develop this research work.

Author contribution Claudio Leone: supervision, conceptualisation, investigation, material production, material characterisation, methodology development, formal analysis, writing–review and editing. Emanuele Mingione: methodology development, investigation, measurement, data acquisition, writing–review and editing. Silvio Genna: material production, material characterisation, investigation, review and editing.

Funding Open access funding provided by Università degli Studi della Campania Luigi Vanvitelli within the CRUI-CARE Agreement. This study was partially supported by an academic grant (Funding program VALERE assigned to Emanuele Mingione) from the University of Campania Luigi Vanvitelli.

Declarations

Ethics approval The manuscript has not been submitted to more than one journal for simultaneous consideration. The manuscript has not been published previously. The study was not split up into several parts. The data have not been fabricated or manipulated to support our conclusions. No data, text, or theories by others are presented as if they were the authors' own. Consent to submit has been received from all co-authors and responsible authorities at the institute/organisation where the work has been carried out before the work is submitted. Authors whose names appear on the submission have contributed sufficiently to the scientific work and therefore share collective responsibility and accountability for the results.

Consent to participate Not applicable.

Consent for publication Not applicable.

Competing interests The authors declare no competing interests.

Open Access This article is licensed under a Creative Commons Attribution 4.0 International License, which permits use, sharing, adaptation, distribution and reproduction in any medium or format, as long as you give appropriate credit to the original author(s) and the source, provide a link to the Creative Commons licence, and indicate if changes were made. The images or other third party material in this article are included in the article's Creative Commons licence, unless indicated otherwise in a credit line to the material. If material is not included in the article's Creative Commons licence and your intended use is not permitted by statutory regulation or exceeds the permitted use, you will need to obtain permission directly from the copyright holder. To view a copy of this licence, visit <http://creativecommons.org/licenses/by/4.0/>.

References

1. Witten E, Mathes V, Sauer M, Kühnel M (2018) AVK market report: composites market report 2018. https://www.avk-tv.de/files/20181115_avk_ccev_market_report_2018_final.pdf. Accessed 22 Jun 2021
2. Carbon fiber market by raw material, fiber type, product type, modulus, application, end-use. https://www.marketsandmarkets.com/Market-Reports/carbon-fiber-396.html?gclid=EAIAIQobChMItZGHi-Cq8QIVkACLCh3D8QqGEAAYASAAEgIONPD_BwE. Accessed 22 Jun 2021
3. Pickering SJ, Turner TA (2014) Research and development in support of carbon fibre recycling. In: Proceedings of CAMX2014-composites and advanced materials expo: combined strength unsurpassed innovation. Orlando, USA

4. Halliwell S (2010) FRPs - The environmental agenda. *Adv Struct Eng* 13:783–791. <https://doi.org/10.1260/1369-4332.13.5.783>
5. Witik RA, Teuscher R, Michaud V et al (2013) Carbon fibre reinforced composite waste: an environmental assessment of recycling, energy recovery and landfilling. *Compos Part A Appl Sci Manuf* 49:89–99. <https://doi.org/10.1016/j.compositesa.2013.02.009>
6. Naqvi SR, Prabhakara HM, Bramer EA et al (2018) A critical review on recycling of end-of-life carbon fibre/glass fibre reinforced composites waste using pyrolysis towards a circular economy. *Resour Conserv Recycl* 136:118–129. <https://doi.org/10.1016/j.resconrec.2018.04.013>
7. Kumar S, Krishnan S (2020) Recycling of carbon fiber with epoxy composites by chemical recycling for future perspective: a review. *Chem Pap* 74:3785–3807
8. Wang B, Wang X, Xu N et al (2021) Recycling of carbon fibers from unsaturated polyester composites via a hydrolysis-oxidation synergistic catalytic strategy. *Compos Sci Technol* 203:108589. <https://doi.org/10.1016/j.compscitech.2020.108589>
9. Bai Y, Wang Z, Feng L (2010) Chemical recycling of carbon fibers reinforced epoxy resin composites in oxygen in supercritical water. *Mater Des* 31:999–1002. <https://doi.org/10.1016/j.matdes.2009.07.057>
10. Hyde JR, Lester E, Kingman S et al (2006) Supercritical propanol, a possible route to composite carbon fibre recovery: a viability study. *Compos Part A Appl Sci Manuf* 37:2171–2175. <https://doi.org/10.1016/j.compositesa.2005.12.006>
11. Yuyan L, Guohua S, Linghui M (2009) Recycling of carbon fibre reinforced composites using water in subcritical conditions. *Mater Sci Eng A* 520:179–183. <https://doi.org/10.1016/j.msea.2009.05.030>
12. Jiang G, Pickering SJ, Lester EH et al (2009) Characterisation of carbon fibres recycled from carbon fibre/epoxy resin composites using supercritical n-propanol. *Compos Sci Technol* 69:192–198. <https://doi.org/10.1016/j.compscitech.2008.10.007>
13. Pickering SJ (2006) Recycling technologies for thermoset composite materials-current status. *Compos Part A Appl Sci Manuf* 37:1206–1215. <https://doi.org/10.1016/j.compositesa.2005.05.030>
14. Kim KW, Lee HM, An JH et al (2017) Recycling and characterization of carbon fibers from carbon fiber reinforced epoxy matrix composites by a novel super-heated-steam method. *J Environ Manag* 203:872–879. <https://doi.org/10.1016/j.jenvman.2017.05.015>
15. Okajima I, Sako T (2019) Recycling fiber-reinforced plastic using supercritical acetone. *Polym Degrad Stab* 163:1–6. <https://doi.org/10.1016/j.polymdegradstab.2019.02.018>
16. Deng J, Xu L, Liu J et al (2020) Efficient method of recycling carbon fiber from the waste of carbon fiber reinforced polymer composites. *Polym Degrad Stab* 182:109419. <https://doi.org/10.1016/j.polymdegradstab.2020.109419>
17. Meyer LO, Schulte K, Grove-Nielsen E (2009) CFRP-recycling following a pyrolysis route: process optimization and potentials. *J Compos Mater*. SAGE Publications/Sage UK, London, England, pp 1121–1132
18. Fernández A, González C, López F et al (2018) Recycling of composites by recovering carbon fibres from prepregs, and their re-usage. *ECCM18 - 18th European Conference on Composite Materials*. Greece, Athens, pp 1–6
19. Cheng H, Sun Y, Wang X et al (2019) Recycling carbon fiber/epoxy resin composites by thermal excitation oxide semiconductors. *Fibers Polym* 20:760–769. <https://doi.org/10.1007/s12221-019-7946-8>
20. Jeong JS, Kim KW, An KH, Kim BJ (2019) Fast recovery process of carbon fibers from waste carbon fibers-reinforced thermoset plastics. *J Environ Manag* 247:816–821. <https://doi.org/10.1016/j.jenvman.2019.07.002>
21. Akbar A, Liew KM (2020) Influence of elevated temperature on the microstructure and mechanical performance of cement composites reinforced with recycled carbon fibers. *Compos Part B Eng* 198:108245. <https://doi.org/10.1016/j.compositesb.2020.108245>
22. Abdou TR, Botelho Junior AB, Espinosa DCR, Tenório JAS (2021) Recycling of polymeric composites from industrial waste by pyrolysis: deep evaluation for carbon fibers reuse. *Waste Manag* 120:1–9. <https://doi.org/10.1016/j.wasman.2020.11.010>
23. Hadigheh SA, Wei Y, Kashi S (2021) Optimisation of CFRP composite recycling process based on energy consumption, kinetic behaviour and thermal degradation mechanism of recycled carbon fibre. *J Clean Prod* 292:125994. <https://doi.org/10.1016/j.jclepro.2021.125994>
24. Liu Y, Farnsworth M, Tiwari A (2017) A review of optimisation techniques used in the composite recycling area: state-of-the-art and steps towards a research agenda. *J Clean Prod* 140:1775–1781. <https://doi.org/10.1016/j.jclepro.2016.08.038>
25. Saccani A, Manzi S, Lancellotti I, Lippardini L (2019) Composites obtained by recycling carbon fibre/epoxy composite wastes in building materials. *Constr Build Mater* 204:296–302. <https://doi.org/10.1016/j.conbuildmat.2019.01.216>
26. Akbar A, Liew KM (2020) Assessing recycling potential of carbon fiber reinforced plastic waste in production of eco-efficient cement-based materials. *J Clean Prod* 274:123001. <https://doi.org/10.1016/j.jclepro.2020.123001>
27. Xiong C, Lan T, Li Q et al (2020) Study of mechanical properties of an eco-friendly concrete containing recycled carbon fiber reinforced polymer and recycled aggregate. *Materials (Basel)* 13:1–16. <https://doi.org/10.3390/ma13204592>
28. Xiong C, Li Q, Lan T et al (2021) Sustainable use of recycled carbon fiber reinforced polymer and crumb rubber in concrete: mechanical properties and ecological evaluation. *J Clean Prod* 279:123624. <https://doi.org/10.1016/j.jclepro.2020.123624>
29. Bledzki AK, Seidlitz H, Krenz J et al (2020) Recycling of carbon fiber reinforced composite polymers—review—part 2: Recovery and application of recycled carbon fibers. *Polymers (Basel)* 12:1–10
30. Genna S, Papa I, Lopresto V, Tagliaferri V (2020) Mechanical characterisation of CFRP laminates with recycled carbon fiber obtained by resin infusion under Flexible Tooling (RIFT) technology. *Compos Sci Technol* 199:108328. <https://doi.org/10.1016/j.compscitech.2020.108328>
31. David F, Tagliaferri V, Trovalusci F (2021) CFRP laminates with recycled carbon fiber: resin infusion and mechanical characterisation. *Mater Sci Forum* 1046:111–117. <https://doi.org/10.4028/WWW.SCIENTIFIC.NET/MSF.1046.111>
32. Abrate S, Walton DA (1992) Machining of composite materials. Part I: Traditional methods *Compos Manuf* 3:75–83. [https://doi.org/10.1016/0956-7143\(92\)90119-F](https://doi.org/10.1016/0956-7143(92)90119-F)
33. Teti R (2002) Machining of composite materials. *CIRP Ann - Manuf Technol* 51:611–634. [https://doi.org/10.1016/S0007-8506\(07\)61703-X](https://doi.org/10.1016/S0007-8506(07)61703-X)
34. Ramulu M (1997) Machining and surface integrity of fibre-reinforced plastic composites. *Sadhana* 22:449–472. <https://doi.org/10.1007/BF02744483>
35. Abrate S, Walton D (1992) Machining of composite materials. Part II: Non-traditional methods *Compos Manuf* 3:85–94. [https://doi.org/10.1016/0956-7143\(92\)90120-J](https://doi.org/10.1016/0956-7143(92)90120-J)
36. Shanmugam DK, Nguyen T, Wang J (2008) A study of delamination on graphite/epoxy composites in abrasive waterjet machining. *Compos Part A Appl Sci Manuf* 39:923–929. <https://doi.org/10.1016/j.compositesa.2008.04.001>
37. Gropetti R, Armanni A, Cattaneo A, Franceschini G (1992) Contribution to the study of the delamination of carbon fibre reinforced plastic (CFRP) laminated composites during piercing and cutting by hydro jet machining (HJM) and hydro abrasive jet

- machining (HAJM). *Comput Aided Des Compos Mater Technol* III:189–209
38. Shanmugam DK, Chen FL, Siores E, Brandt M (2002) Comparative study of jetting machining technologies over laser machining technology for cutting composite materials. *Compos Struct* 57:289–296. [https://doi.org/10.1016/S0263-8223\(02\)00096-X](https://doi.org/10.1016/S0263-8223(02)00096-X)
 39. Leone C, Genna S, Caggiano A et al (2016) Influence of process parameters on kerf geometry and surface roughness in Nd:YAG laser cutting of Al 6061T6 alloy sheet. *Int J Adv Manuf Technol*. <https://doi.org/10.1007/s00170-016-8667-4>
 40. Leone C, Genna S, Tagliaferri V (2018) Cutting of AA6061 by a multimode pulsed Nd:YAG laser with high pressure gas: characterisation of kerf geometry and quality. *Int J Adv Manuf Technol*. <https://doi.org/10.1007/s00170-017-0804-1>
 41. Karatas C, Keles O, Uslan I, Usta Y (2006) Laser cutting of steel sheets: influence of workpiece thickness and beam waist position on kerf size and stria formation. *J Mater Process Technol* 172:22–29. <https://doi.org/10.1016/j.jmatprotec.2005.08.017>
 42. Fomin VM, Golyshov AA, Malikov AG et al (2015) Mechanical characteristics of high-quality laser cutting of steel by fiber and CO2 lasers. *J Appl Mech Tech Phys* 56:726–735. <https://doi.org/10.1134/S0021894415040203>
 43. Rodrigues GC, Vorkov V, Dufflou JR (2018) Optimal laser beam configurations for laser cutting of metal sheets. In: *Procedia CIRP*. Elsevier B.V., pp 714–718
 44. Genna S, Menna E, Rubino G, Tagliaferri V (2020) Experimental investigation of industrial laser cutting: the effect of the material selection and the process parameters on the kerf quality. *Appl Sci* 10:4956. <https://doi.org/10.3390/app10144956>
 45. Tamilarasan A, Rajamani D (2017) Multi-response optimization of Nd:YAG laser cutting parameters of Ti-6Al-4V superalloy sheet. *J Mech Sci Technol* 31:813–821. <https://doi.org/10.1007/s12206-017-0133-1>
 46. Tönshoff HK, Emmelmann C (1989) Laser cutting of advanced ceramics. *CIRP Ann - Manuf Technol* 38:219–222. [https://doi.org/10.1016/S0007-8506\(07\)62689-4](https://doi.org/10.1016/S0007-8506(07)62689-4)
 47. Quintero F, Pou J, Lusquinos F et al (2001) Nd:YAG laser cutting of advanced ceramics. In: *4th Iberoamerican Meeting on Optics and 7th Latin American Meeting on Optics, Lasers, and Their Applications*. SPIE, pp 756–760
 48. Yan Y, Ji L, Bao Y et al (2013) CO2 laser high-speed crack-free cutting of thick-section alumina based on close-piercing lapping technique. *Int J Adv Manuf Technol* 64:1611–1624. <https://doi.org/10.1007/s00170-012-4127-y>
 49. Yilbas BS, Khan S, Raza K et al (2010) Laser cutting of 7050 Al alloy reinforced with Al₂O₃ and B₄C composites. *Int J Adv Manuf Technol* 50:185–193. <https://doi.org/10.1007/s00170-009-2489-6>
 50. Mathew J, Goswami GL, Ramakrishnan N, Naik NK (1999) Parametric studies on pulsed Nd:YAG laser cutting of carbon fibre reinforced plastic composites. *J Mater Process Technol* 89–90:198–203. [https://doi.org/10.1016/S0924-0136\(99\)00011-4](https://doi.org/10.1016/S0924-0136(99)00011-4)
 51. Weber R, Hafner M, Michalowski A, Graf T (2011) Minimum damage in CFRP laser processing. *Phys Procedia* 12:302–307. <https://doi.org/10.1016/j.phpro.2011.03.137>
 52. Riveiro A, Quintero F, Lusquinos F et al (2012) Experimental study on the CO2 laser cutting of carbon fiber reinforced plastic composite. *Compos Part A Appl Sci Manuf* 43:1400–1409. <https://doi.org/10.1016/j.compositesa.2012.02.012>
 53. Gautam GD, Mishra DR (2019) Firefly algorithm based optimization of kerf quality characteristics in pulsed Nd:YAG laser cutting of basalt fiber reinforced composite. *Compos Part B Eng* 176:107340. <https://doi.org/10.1016/j.compositesb.2019.107340>
 54. Jain A, Singh B, Shrivastava Y (2019) Reducing the heat-affected zone during the laser beam drilling of basalt-glass hybrid composite. *Compos Part B Eng* 176:107294. <https://doi.org/10.1016/j.compositesb.2019.107294>
 55. Bluemel S, Jaeschke P, Wippo V et al (2012) Laser machining of CFRP using a high power fiber laser - Investigations on the heat affected zone. In: *ECCM 2012 - Composites at Venice, Proceedings of the 15th European Conference on Composite Materials*. Venice, Italy, pp 1–8
 56. Cenna AA, Mathew P (2002) Analysis and prediction of laser cutting parameters of fibre reinforced plastics (FRP) composite materials. *Int J Mach Tools Manuf* 42:105–113. [https://doi.org/10.1016/S0890-6955\(01\)00090-6](https://doi.org/10.1016/S0890-6955(01)00090-6)
 57. Pan CT, Hocheng H (1996) The anisotropic heat-affected zone in the laser grooving of fiber-reinforced composite material. *J Mater Process Technol* 62:54–60. [https://doi.org/10.1016/0924-0136\(95\)02192-2](https://doi.org/10.1016/0924-0136(95)02192-2)
 58. Sheng P, Chryssolouris G (1995) Theoretical model of laser grooving for composite materials. *J Compos Mater* 29:96–112. <https://doi.org/10.1177/002199839502900105>
 59. Goeke A, Emmelmann C (2010) Influence of laser cutting parameters on CFRP part quality. In: *Physics Procedia*. Elsevier B.V., pp 253–258
 60. Herzog D, Schmidt-Lehr M, Canisius M et al (2015) Laser cutting of carbon fiber reinforced plastic using a 30 kW fiber laser. *J Laser Appl* 27:S28001. <https://doi.org/10.2351/1.4906304>
 61. Chryssolouris G (1991) *Laser machining: theory and practice* New York
 62. Leone C, Genna S, Tagliaferri V (2014) Fibre laser cutting of CFRP thin sheets by multi-passes scan technique. *Opt Lasers Eng* 53:43–50. <https://doi.org/10.1016/j.optlaseng.2013.07.027>
 63. Leone C, Pagano N, Lopresto V, De Iorio I (2009) Solid state Nd:YAG laser cutting of CFRP sheet: influence of process parameters on kerf geometry and HAZ. In *ICCM International Conferences on Composite Materials*
 64. Leone C, Genna S (2018) Heat affected zone extension in pulsed Nd:YAG laser cutting of CFRP. *Compos Part B Eng*. <https://doi.org/10.1016/j.compositesb.2017.12.028>
 65. Wu CW, Wu XQ, Huang CG (2015) Ablation behaviors of carbon reinforced polymer composites by laser of different operation modes. *Opt Laser Technol* 73:23–28. <https://doi.org/10.1016/j.optlastec.2015.04.008>
 66. Chien CY, Gupta MC (2005) Pulse width effect in ultrafast laser processing of materials. *Appl Phys A Mater Sci Process* 81:1257–1263. <https://doi.org/10.1007/s00339-004-2989-z>
 67. Lau WS, Lee WB, Pang SQ (1990) Pulsed Nd: YAG laser cutting of carbon fibre composite materials. *CIRP Ann - Manuf Technol* 39:179–182. [https://doi.org/10.1016/S0007-8506\(07\)61030-0](https://doi.org/10.1016/S0007-8506(07)61030-0)
 68. Takahashi K, Tsukamoto M, Masuno S, Sato Y (2016) Heat conduction analysis of laser CFRP processing with IR and UV laser light. *Compos Part A Appl Sci Manuf* 84:114–122. <https://doi.org/10.1016/j.compositesa.2015.12.009>
 69. Fujita M, Ohkawa H, Somekawa T et al (2016) Wavelength and pulsewidth dependences of laser processing of CFRP. In *Physics Procedia*. Elsevier B.V., pp 1031–1036
 70. Wolynski A, Herrmann T, Mucha P et al (2011) Laser ablation of CFRP using picosecond laser pulses at different wavelengths from UV to IR. *Phys Procedia* 12:292–. <https://doi.org/10.1016/j.phpro.2011.03.136>
 71. G C, Candelieri T, Querci L et al (2013) Method and apparatus for manufacturing of non-woven fabric from recycled carbon fibers and the non-woven fabric so formed
 72. *Karborek Recycling Carbon Fibres*. http://www.karborekrcf.it/index_eng.html. Accessed 28 Jun 2021
 73. Ready JF, Farson DF, Feeley T (2001) *LIA handbook of laser materials processing*. Springer-Verlag, Berlin Heidelberg, New York

74. ASTM International (2014) ASTM D 3039/D 3039M-14 standard test method for tensile properties of polymer matrix composite materials. ASTM B Stand
75. ASTM International (2017) ASTM D 790–17-standard test method for flexural properties of unreinforced and reinforced plastics and electrical insulation materials. ASTM Stand
76. ASTM International (2020) ASTM D 792–20 standard test methods for density and specific gravity (relative density) of plastics. Annu B ASTM Stand
77. ASTM International (2015) ASTM D 3171–15 - standard test methods for constituent content of composite materials. ASTM B Stand
78. Montgomery DC (2019) Design and analysis of experiments, 10th edn. Wiley, New York, NY
79. Coleman DE, Montgomery DC (1993) A systematic approach to planning for a designed industrial experiment. *Technometrics* 53:1–12. <https://doi.org/10.1080/00401706.1993.10484984>
80. Leone C, Mingione E, Genna S (2021) Laser cutting of CFRP by quasi-continuous wave (QCW) fibre laser: effect of process parameters and analysis of the HAZ index. *Compos Part B Eng* 224:109146. <https://doi.org/10.1016/J.COMPOSITESB.2021.109146>
81. Li M, Li S, Yang X et al (2018) Fiber laser cutting of CFRP laminates with single- and multi-pass strategy: a feasibility study. *Opt Laser Technol* 107:443–453. <https://doi.org/10.1016/j.optlastec.2018.06.025>
82. Li M, Li S, Yang X et al (2019) Effect of lay-up configuration and processing parameters on surface quality during fiber laser cutting of CFRP laminates. *Int J Adv Manuf Technol* 100:623–635. <https://doi.org/10.1007/s00170-018-2728-9>
83. Rao S, Sethi A, Das AK et al (2017) Fiber laser cutting of CFRP composites and process optimization through response surface methodology. *Mater Manuf Process* 32:1612–1621. <https://doi.org/10.1080/10426914.2017.1279296>
84. Tagliaferri V, Visconti IC (1987) Machining of fibre reinforced materials with laser beam: cut quality evaluation. In: *Proceedings of European conference on composite materials*. Elsevier, London, UK, pp 190–199
85. Jovane F, Di Ilio A, Tagliaferri V, Veniali F (1993) Laser machining of composite materials. In: Martellucci S, Chester AN, Scheggi AM (eds) *Laser applications for mechanical industry*, NATO ASI S. Springer, Dordrecht, The Netherlands, pp 115–129

Publisher's note Springer Nature remains neutral with regard to jurisdictional claims in published maps and institutional affiliations.